Doctoral Dissertation

Structural and Mechanistic Insight into a Novel Enoate Reductase in Fatty-acid Metabolism Pathway

（脂肪酸代謝経路における新規エノン還元酵素の構造と機能の解明）

Feng Hou

侯 峰

Table of contents

Abbreviations

CBB	coomassie brilliant blue
DTT	dithiothreitol
DNA	deoxyribonucleic acid
E.coli	*Escherichia coli*
FMN	flavin mononucleotide (oxidized form)
$FMNH^-$	flavin mononucleotide (reduced form)
GI-tract	gastrointestinal-tract
IPTG	isopropyl β-D-1-thiogalactopyranoside
KetoB	10-oxo-*trans*-11-octadecenoic acid (substrate)
KetoC	10-oxooctadecanoic acid (product)
LB	lysogeny broth
MWCO	molecular weight cut-off
NADH	nicotinamide adenine dinucleotide (reduced form)
OYE	old yellow enzyme
PCR	polymerase chain reaction
PDB	protein data bank
PEG	polyethylene glycol
PPAR	peroxisome proliferation-activated receptor
RMSD	root mean square deviation
SDS-PAGE	sodium dodecyl sulfate-polyacrylamide gel electrophoresis

Abstract

In a living organism, fatty acids serve many essential functions. They can be remodeled by elongation, insertion or removal of double bonds. Several metabolic pathways have been discovered and studied to investigate the mechanism of the reactions and the regulation of fatty acids. Generally, fatty acids are activated by combined with CoA or ACP before modification. Recently, a novel saturation pathway of linoleic acid was discovered from *Lactobacillus plantarum* AKU 1009a, which consists of reactions utilizing fatty acids without CoA or ACP as substrate. Among the enzymes constituting the pathway, CLA-ER was identified as an enoate reductase and to saturate the C=C bond of 10-oxo-*trans*-11-octadecenoic acid (KetoB) to generate oxooctadecanoic acid (KetoC). Based on the amino-acid sequence, CLA-ER is concluded to belong to the NADH oxidase/flavin reductase family. However, no enzyme has been reported to show an enoate reduction activity in this family before. Here, I report the crystal structures of CLA-ER in both the holoenzyme state and KetoC-bound state, which elucidate the novel reaction mechanism and the structural basis of substrate recognition.

CLA-ER forms a homodimeric structure. A CLA-ER molecule can be divided into two subdomains, core subdomain and flexible subdomain. Superposition of the structures in two states reveals the almost same conformation of the core subdomain. However, a significant conformational change was observed at the flexible subdomain. In KetoC-free state, CLA-ER adopts an open form with an exposure of the groove for preliminary recognition of fatty acids. The groove consists of a positive charge half and a hydrophobic half, which contributes to fatty acid orientation. Upon the fatty acid binding, the flexible subdomain rotates about 45 deg towards the core subdomain of the other protomer in dimer. The flexible subdomain acts as a “cap”, which captures a fatty acid when it has been preliminarily recognized by the groove. The conformational change of the “cap” structure makes CLA-ER change to it closed

form and results in the formation of the binding site for fatty-acid recognition and reaction. Both the open-closed transformation mechanism and the charge distribution in fatty acid binding groove are considered to enable CLA-ER to recognize fatty acid without CoA or ACP.

Furthermore, based on structural analyses and enzyme assays, I also identified C51, Y101 and F126 as the critical residues for catalytic activity and proposed the catalytic mechanism of CLA-ER. In the binding site, the enone group of substrate is recognized by C51 and FMN through hydrogen bonds, and spatial rearrangement of F126. The C=C bond of KTB was saturated by accepting hydride from $FMNH^-$ and proton from Y101 via C51. However, KTB can also be reduced by C51A mutation, which suggests there is another candidate pathway for electron transfer. Structure of CLA-ER indicates that electron may be transferred through the peptide bond between C51 and A50 to solvent. Structural comparison and sequence alignment of some enzymes belonging to NADH oxidase/FMN reductase family indicate that the “cap” structure, the hydrophobic “key” (F126) and the catalytic cysteine and tyrosine residues are the structural features that make CLA-ER identified as enoate reductase preferentially.

Chapter 1

Introduction

1.1 Fatty acid

In living organism, fatty acids exist as constituents of neutral and polar lipids, side chains in some coenzymes and secondary metabolites, covalent attachments to distinct eukaryotic proteins, and parts of eucaryotic second-messenger molecules and serve many essential functions. Due to the important roles of fatty acids, researches on fatty acids, relative proteins and pathways have been extensively performed. For example, intracellular lipid chaperones, known as fatty acid binding proteins (FABPs), have been demonstrated to coordinate lipid responses, metabolic and inflammatory pathway. FABPs may actively facilitate the transport of lipids to the lipid droplet for storage; to other enzymes to regulate their activity; to the endoplasmic reticulum for signaling and membrane synthesis; to the nucleus for lipid-mediated transcriptional regulation; to the mitochondria or peroxisome for oxidation; or even outside the cell to signal in an autocrine or paracrine manner (1-5) (Fig. 1-1). Some FABPs have been demonstrated to be vital to human health. Such as adipocyte/macrophage FABPs, A-FABP and E-FABP (also known as FABP4 and FABP5, respectively) have a central role in many aspects of metabolic diseases including obesity, diabetes and atherosclerosis (6-8). Especially, convincing evidence has been presented that A-FABP, the best-characterized isoform among the FABP family, promotes insulin resistance, hypertriacylglyceroalemia and atherosclerosis (9). Therefore, targeting these FABPs is considered to offer highly attractive therapeutic opportunities for a broad range of pathologies in metabolic diseases.

In another aspect, researches on fatty acids reveal fatty acids with different formation serve distinct functions in physiology. Triacylglycerols and cholesteryls ester are involved in biological energy storage; phospholipids, plasmalogens and sphingolipids are involved in the structural integrity and dynamics; diacylglycerols, phosphatidylinositols and eicosanoids are involved in the control of cellular metabolism and cell physiology (10, 11). Due to diversity of fatty acids and the distinct functions of fatty acids in different formations, the regulation of

fatty acid composition will also have important ramification to human health.

1.2 Fatty acid modification pathway

In living organism, fatty acid can be remodeled by elongation, insertion or removal of double bonds or covalently bound to proteins, converted to alcohols or aldehydes, and degraded for energy production. Amount of enzymes involved in these pathways have been discovered and studied to investigate their mechanism. As a common initial step of all the metabolic processes of fatty acids, thioesterification of fatty acids with coenzyme A (CoA) is catalyzed by the acyl-coenzyme A synthetases (ACSs) to generate activated intermediates (12) (Fig. 1-2). The thioester bond has very high energy, which make it unstable and easily transferred to other molecules. The activated acyl-CoAs generated from the reactions are used to the following pathways, such as complex lipid synthesis, energy production, protein acylation and fatty acid dependent transcriptional regulation. For example, fatty acid synthesis proceeds by the addition of two carbon units from malonyl-CoA. Elongation up to 16 carbons in length undergoes a well-defined multiple step pathway and is catalyzed by fatty acid synthase (FAS) which is various in the molecular structure from different source but essentially share the same reaction mechanism in all biological systems (13-16). Synthesis of fatty acid by FAS is initiated by condensation of a primer with two carbon units donated from malonyl-ACP (Acyl carrier protein), which is generated from malonyl-CoA (Fig. 1-3). Following the condensation, the β-keto group is reduced to the saturated carbon chain by the sequential action of a ketoreductase, dehyratase and enoate reductase (17) (Fig. 1-3). Further elongation into long chain fatty acids containing 18 carbon atoms or longer are performed in endoplasmic reticulum with enzymatic steps principally the same as described for FAS, but using malonyl-CoA as the carrier of acyl chain (18) (Fig. 1-3).

1.3 Novel saturation pathway in *Lactobacillus plantarum* AKU 1009a

Recently, a novel linoleic acid saturation pathway was identified during a study on conjugated fatty acid synthesis in gut bacteria. By the pathway, *Lactobacillus plantarum* AKU1009a (AKU Culture collection, Faculty of Agriculture, Kyoto University) tranforms *cis*-9,*cis*-12 diene structure of C18 fatty acid, such as linoleic acid, α-linolenic acid and γ-linolenic acid into the conjugated diene structures *cis*-9,*trans*-11 and *trans*-9,*trans*-11 (19-23),or saturates these conjugated dienes into the *trans*-10 monoene (24). Interestingly, enzymes involved in this pathway catalyze reactions on free fatty acids but not CoA- or ACP-activated fatty acids,

The linoleic acid saturation pathway consists of four enzymes. The first enzyme, termed CLA-HY, catalyzes hydration of C=C double bond and its reverse reaction (Fig. 1-4). The second enzyme is a carbonyl reductase/ hydroxyl oxidase, termed CLA-DH, which catalyzed dehydrogenation of hydroxyl group or hydrogenation of carbonyl group at C10 (Fig. 1-4). The third reaction is catalyzed by CLA-DC, a C=C double bond isomerase. The C=C double bond at Δ12 is shift to Δ11, generating the conjugated enone structure, 10-oxo-*trans*-11-fatty acid (Fig. 1-4). The last enzyme is an enoate reductase, termed CLA-ER. The enone structure generated from the third reaction is reduced by CLA-ER, to generate 10-hydroxy fatty acid. These enzymes are also found in other *Lactobacillus* species, such as *L. casei* and *L. rhamnosus*. Furthermore, many other species of lactic acid bacteria also conserve one or more genes of these four enzymes. The conservation of genes makes the saturation pathway more fascinating. Studies on the pathway may provide us a better understanding on the fatty acid metabolism in lactic acid bacteria.

1.4 *Lactobacillus plantarum* and human health.

Microorganisms in the gastrointestinal-tract (GI-tract) interact with their host in many ways and contribute significantly to the maintenance of host health (25). Saturation mechanism by gastrointestinal microbes, such as lactic acid bacteria, is known as a detoxifying mechanism, which transforms growing inhibiting free polyunsaturated fatty acids into less toxic saturated fatty acids (26). The largest group of lactic acid bacteria belongs to the genus of *Lactobacillus*, which contains more than 50 different species (27, 28). *L. plantarum* is commonly found in the human GI-tract and a variety of *L. plantarum* strains are presently marketed as probiotics. Effect of *L. plantarum* consumption on human health has also been studied. A significant increase in the total faecal concentration of carboxylic acids, acetic acids, and propionic acids was found in a study, in which the healthy subjects consumed *L. plantarum* 229V daily for 3 weeks. It indicates that consumption of *L. plantarum* 229V affect the fatty acid metabolism in the subjects (29). Considerable attention has also been given to immune stimulation by *L. plantarum* strains (30). Considering these effects on human health, the development of *L. plantarum* as a living vaccine is considered to offer a large range of therapeutic possibilities.

Within the linoleic acid saturation pathway discovered in *L. plantarum* AKU1009a, several fatty acids have been identified as products or intermediates. Conjugated fatty acids, *cis*-9,*trans*-11-CLA and *trans*-10,*cis*-12-CLA, can be synthesized by the combined reaction of CLA-HY, CLA-DH and CLA-DC. Oleic acid can also be synthesized by the addition of CLA-ER. Studies on both CLA and oleic acid reveal that they both have significant effect on human health. CLA can reduce carcinogenesis, atheroschlerosis and body fat (31-33) and commercialized as a functional food for control of body weight; oleic acid may be responsible for the hypotensive effects of olive oil (34). Otherwise, modified fatty acids with a *trans* conformation or hydroxyl and oxo group can also be generated as intermediates. Consumption of *trans*-fatty acids is considered to increase the risk of coronary heart disease by increasing LDL and reducing HDL cholesterol levels (35). Hydroxyl and oxo-fatty acids act as ligands for PPARγ (36); oxo-fatty acids are also considered to be potent PPARα

activators and decrease the amount of triacylglycerol in obese diabetic mice (37). Thus, the synthesis of these fatty acids in lactic acid bacteria may have significant influence on the health of its host and the regulation of these reactions can be expected to contribute to human health by controlling the composition of these fatty acids.

1.5 CLA-ER and NADH oxidase/flavin reductase family

Structure information is always considered to accelerate chemical compound design for the protein regulation and mutant design for higher productivity. However, all these four enzymes are lack of structure and the reaction mechanism are also rarely studied.

My work focused on CLA-ER, which can saturate the C=C double bond in the 10-oxo-*trans*-11-octadecenoic acid (KetoB) to generate 10-oxooctadecanoic acid (KetoC) (Fig. 1-4). Based on the amino acid sequence, CLA-ER was concluded to belong to the NADH oxidase/flavin reductase family. Enzymes belonging to this family were reported with several functions. The majority of these proteins were reported to catalyze the reduction of flavins by the two electrons transfer from NAD(P)H and most of them are also identified as an nitroreductase via a ping pang Bi Bi mechanism (Fig. 1-5) (38, 39). Enzymes in this family are also reported to take other activities, such as IYD, an iodotyrosine deiodinase, which can salvage iodide from mono- and diiodotyrosine with a reduced FMN (40) and BluB, which is involved in the biosynthesis of vitamin B12 (41). However, no other enzyme in NADH oxidase/flavin reductase family was reported to show an enoate reduction activity (Fig. 1-6).

1.6 Enoate reductases

Various enoate reductases have been identified with different functions, structures and reaction mechanisms. FabI, an enoate-acyl reductase involved in bacterial type II fatty acid

biosynthesis, reduce the enoate group carried by ACP with NADH as cofactor. FabI is concluded to be a member of short-chain alcohol dehydrogenase/reductase (SDR) superfamily characterized by a catalytic triad of key tyrosine, lysine and serine residues and reduce double bond in the enoate substrate (42) (Fig. 1-7A). FabK, an isozyme of FabI with no sequence or structural similarity, reduces the enoate substrate using NADH and FMN by a separate mechanism (43) (Fig. 1-7B). Old yellow enzymes (OYEs) are also well known as enzymes which catalyze the reduction of α,β-unsaturated aldehyde and ketones by turnover reaction using FMN and NADPH as cofactors. It has been clarified that the reduction proceeds via transfer of hydride to the carbon β to the carbonyl and uptake of a solvent-derived proton at the α position through a tyrosine residue (44) (Fig. 1-7C). Reduction reaction using an oxyanion hole has also been proposed for LovC, a transacting enoyl reductase from lovastatin biosynthesis. Hydride of NADPH is transferred to the alkene group and resulting enolate oxide is stabilized by an oxyanion hole. Then proton transfer from an acid (likely water) completes the reduction (45) (Fig. 1-7D). However, none of these enzymes has a similar structure with enzymes in NADH oxidase/flavin reductase family. The enoate reduction reaction of enzyme in NADH oxidase/flavin reductase family is still difficult to speculate.

1.7 Purpose

In a living organism, fatty acids exist in various states and serve many essential functions. Metabolic pathways involved in fatty acid modification have been discovered and studied to investigate the mechanism of the reactions and the regulation of fatty acids. The novel linoleic acid saturation pathway in *Lactobacillus plantarum* AKU 1009a involves reactions on free fatty acid without CoA or ACP binding and enzymes catalyzing these reactions are extensively conserved in lactic acid bacteria. Within these enzymes, CLA-ER was identified as enoate reductase which saturates the C=C bond of 10-oxo-*trans*-11-octadecenoic acid

(KetoB) to generate oxooctadecanoic acid (KetoC) (Fig. 1-4). Although CLA-ER is concluded to belong to the NADH oxidase/flavin reductase family, no enzyme has been reported to show an enoate reduction activity. Therefore, I report both the substrate-free and substrate-bound structures of CLA-ER, which elucidate the novel reaction mechanism and the structural basis of substrate specificity.

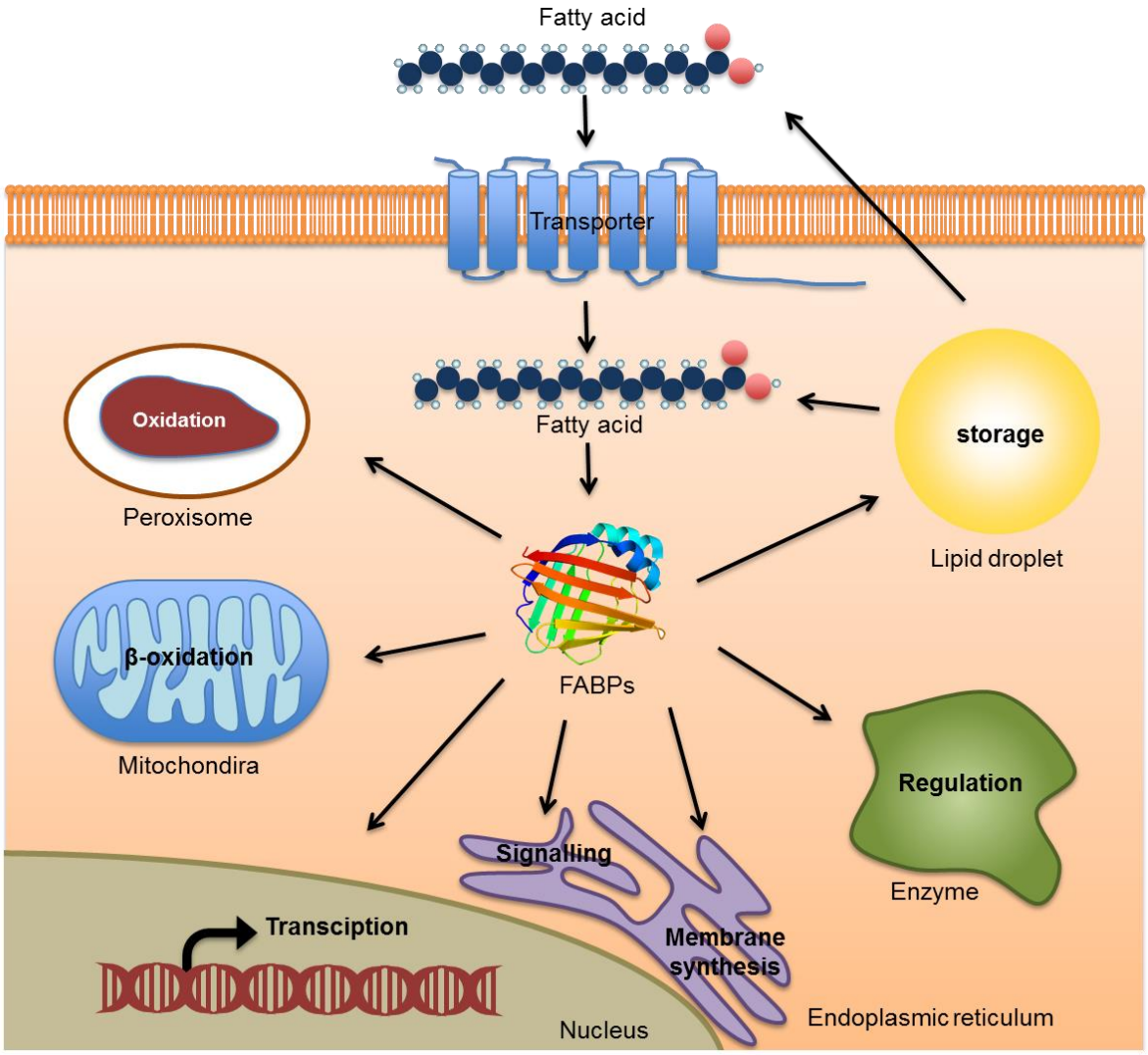

Fig. 1-1 Putative functions of fatty acid through FABPs binding.

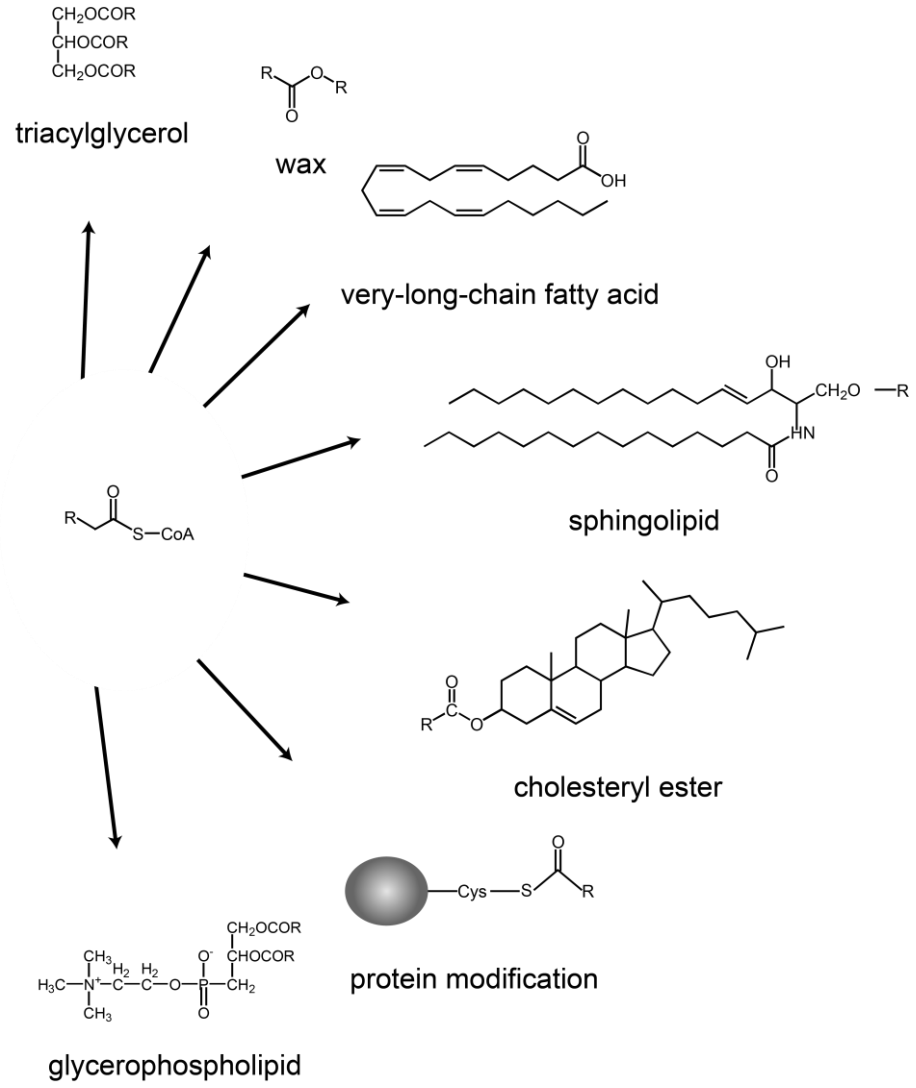

Fig. 1-2 Fatty acid metabolism pathways using acyl-CoA.

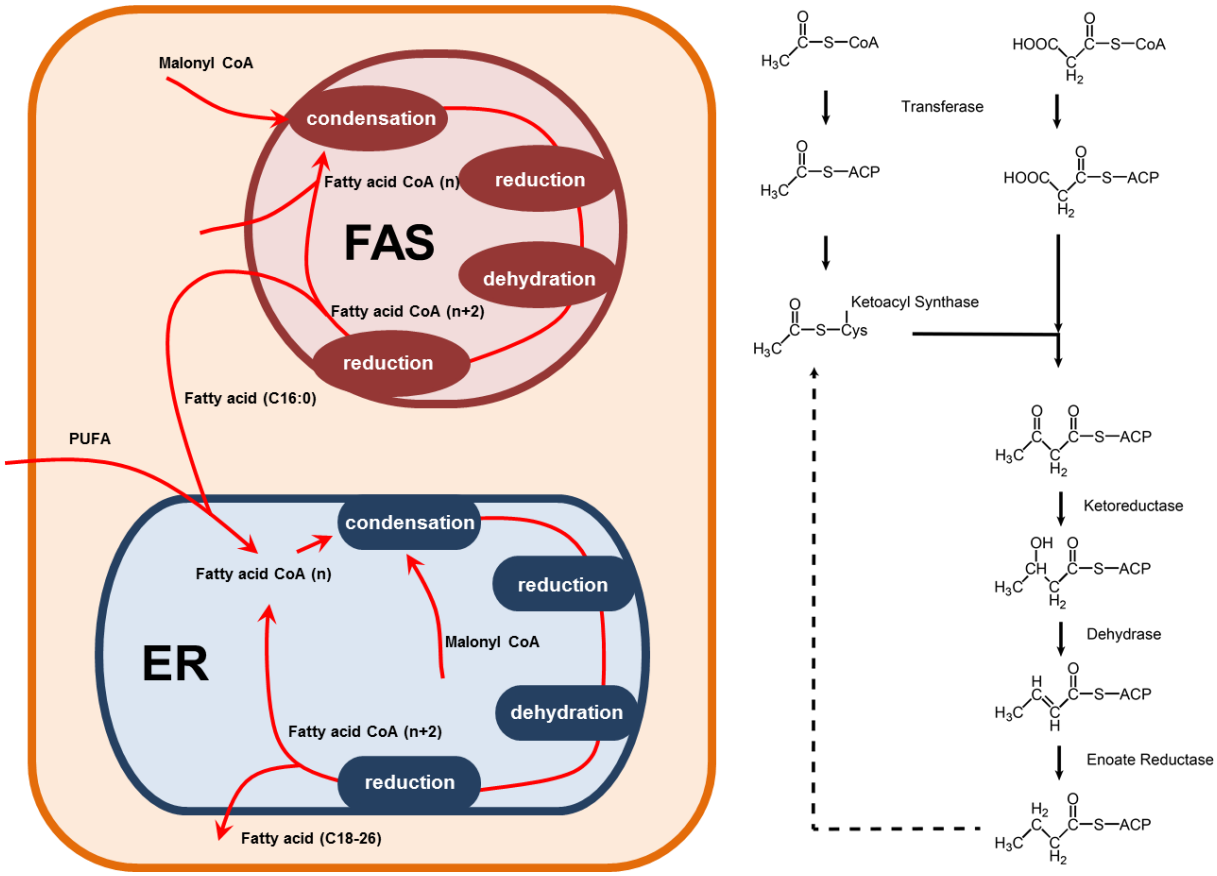

Fig. 1-3 Fatty acid elongation pathways.

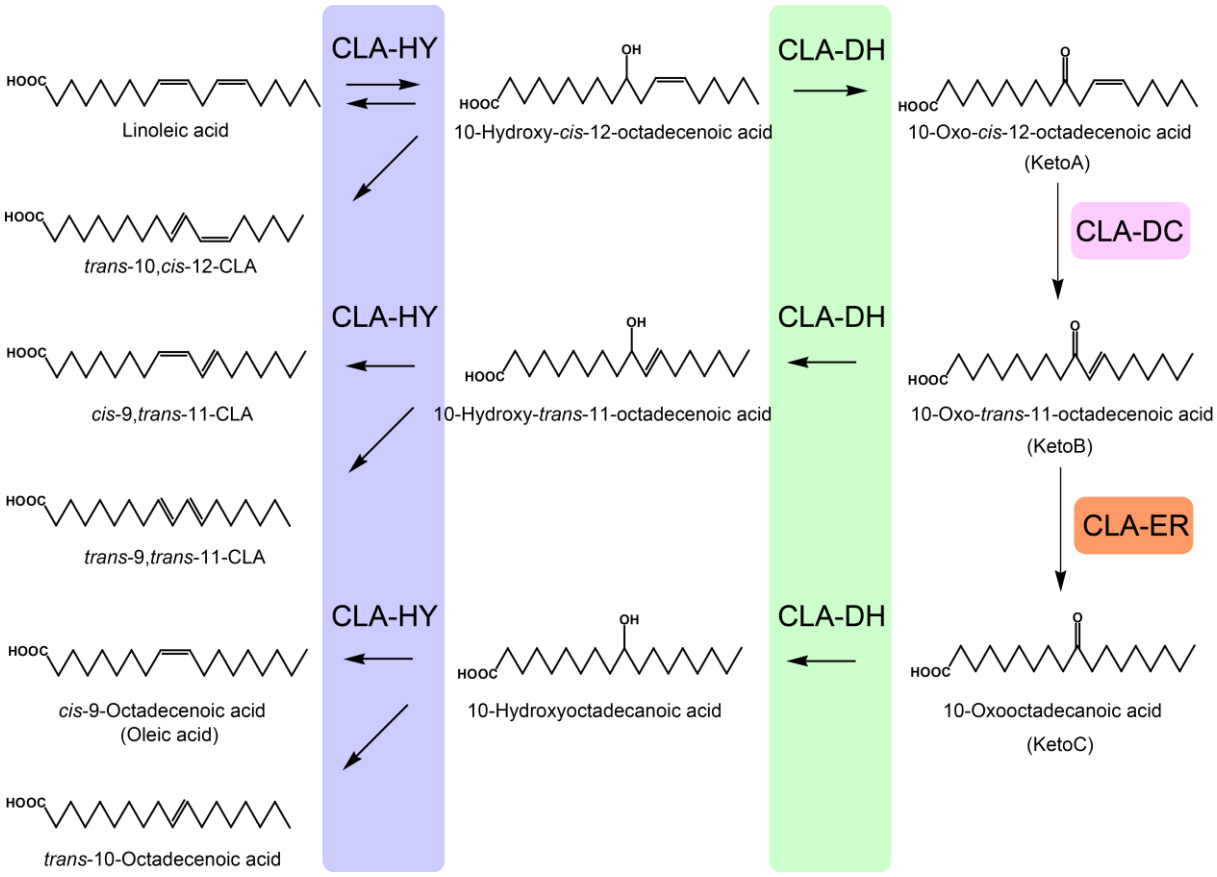

Fig. 1-4 Linoleic acid saturation pathway in *Lactobacillus plantarum* AKU1009a.

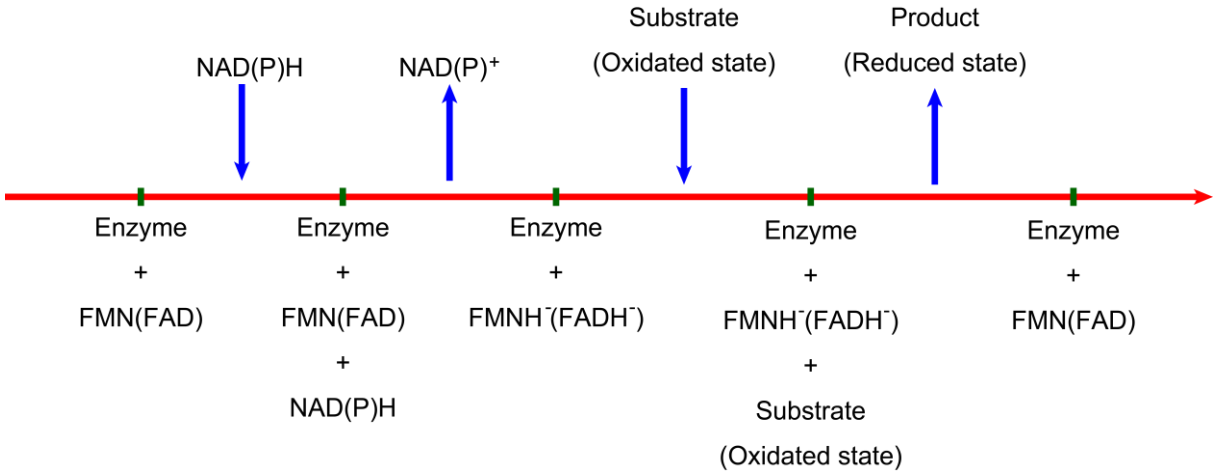

Fig. 1-5 Ping-pong Bi Bi mechanism.

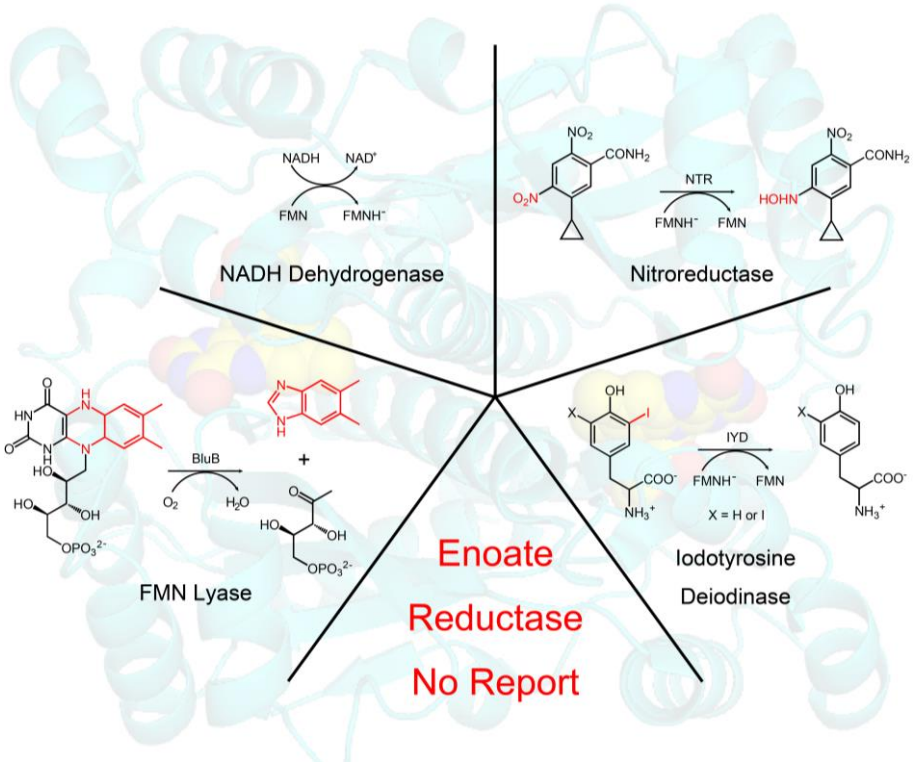

Fig. 1-6 Enzymes belonging to NADH oxidase/flavin reductase family.

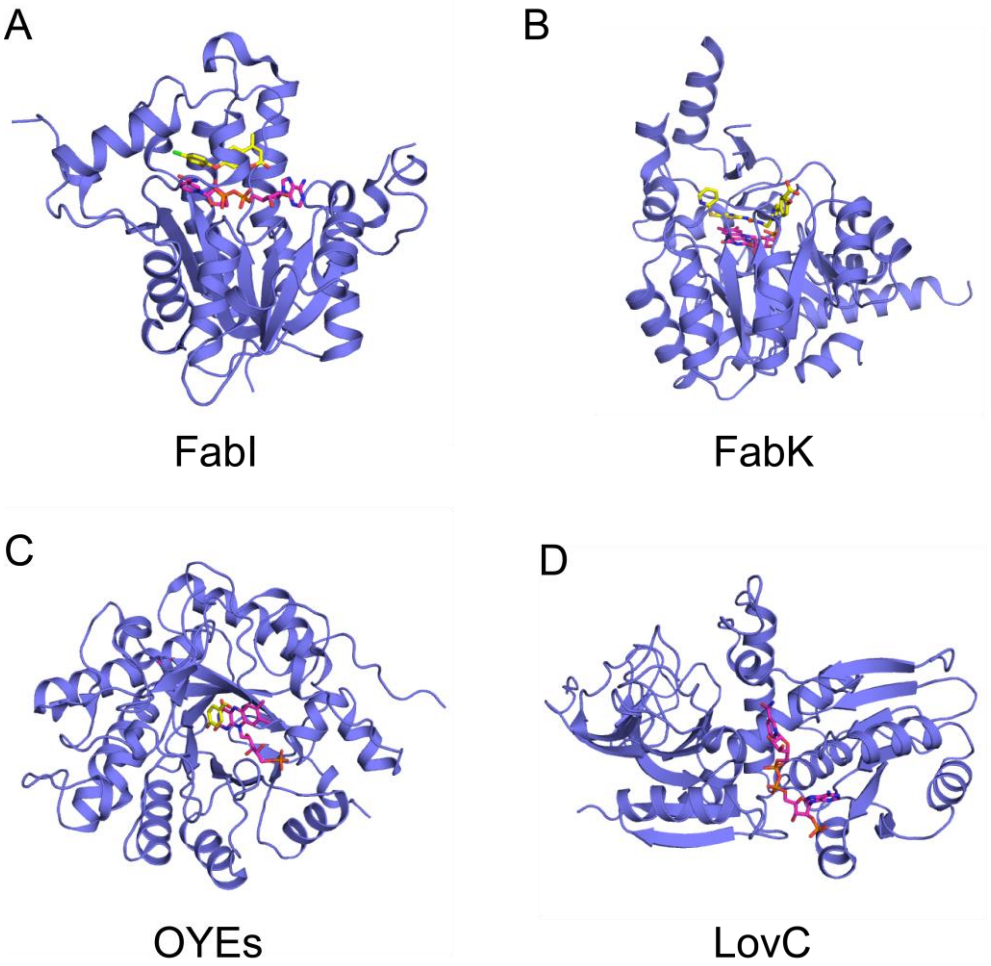

Fig. 1-7 Crystal structures of enoate reductases. Cofactor and inhibitor are indicated by magentas and yellow stick, respectively.

Chapter 2

X-ray Structural Analysis of CLA-ER/FMN

2.1 Exordium

Protein structure is widely used in both science to reveal the functions of biological molecules and industry for drug design or biosynthesis of chemicals. X-ray, NMR, electron microscopy are applied for structural determination at atomic resolution. Among these methods, X-ray crystallography is used most widely. However, a highly ordered protein crystal is necessary for structure determination using X-ray. To obtain a protein crystal, a suitable construct and the high purity of target protein are always considered to be the key point. Besides, protein stabilization is also important for crystallization. Therefore, the temperature, buffer component and additives will also be considered during sample preparation. In this chapter, I will describe cloning, purification, crystallization, structure determination and analysis of CLA-ER in the presence of its cofactor FMN.

2.2 Materials and Methods

2.2.1 Construction of the expression vector

The CLA-ER-coding gene (Genebank accession no. NC_004567; region 60505-61350) was provided by Prof. Ogawa from Kyoto University. Full-length CLA-ER gene was amplified by PCR and inserted into pET-47a(+) vector (Novagen) between the *Sma*I and *Eco*RI sites to produce a recombinant protein with an N-terminal His_6-tag sequence for purification. PCR was performed using PCR system 9700 (Life technologies). The process and primers used for PCR are shown as follows:

Primer	
Forward	5’ - ATGTCAGAAGCAGTGAAAAATTTGGTGAACAATGATTTAG - 3’
Reverse	5’ - CCGGAATTCTCAGGCTAAGAAATCAGTCTGTG - 3’

Reagent composition for PCR	
10×KOD plus buffer	5 μl
dNTPs	5 μl
$MgSO_4$	2 μl
Primers	1.5 μl
Template plasmid	0.5 μl
KOD plus	1 μl
MilliQ	33.5 μl

PCR process			
Step	Temperature (ºC)	Time (sec)	Cycle
First denaturation	94	300	1
Denaturation	94	15	3
Annealing	53.5	30	
Extension	68	60	
Denaturation	94	15	27
Annealing	67	30	
Extension	68	60	
Last Extension	68	300	1

After confirmation by agarose gel electrophoresis, the amplified DNA fragments were purified using the QIAquick PCR Purification Kit (Qiagen). Purified fragments were digested by incubation with restriction endonuclease *Eco*RI (Takara Bio) for 3 h under 310 K. In the meantime, pET-47a(+) plasmids were digested using *Sma*I (Takara Bio) and *Eco*RI. The reagents for reaction are shown as follows:

Restriction endonuclease digestion			
Target DNA fragment		Vector	
DNA fragment	30 μl	Vector	30 μl
10×Buffer H	4 μl	10×Buffer T	4 μl
*Eco*RI	1 μl	BSA	4 μl
MilliQ	5 μl	*Eco*RI	1 μl
		*Sma*I	1 μl

After incubation, the mixture was loaded onto agarose gel for separation. Then Target bonds containing cleaved fragments and cleaved vectors were cut off and the fragments were extracted using the QIAquick Gel Extraction Kit (Qiagen). Next, 2 μl of cleaved CLA-ER-coding DNA fragments, 0.5 μl of cleaved pET-47a(+) plasmids and 2.5 μl of 2×Ligation Mix (Wako) were mixed and incubated for 30 min at 289 K for ligation. After ligation, 2 μl plasmid solution was mixed with 50 μl XL1-Blue competent cell suspension (Stratagene) and incubated on ice for 10 min. Then heat shock was performed at 215K for 45 sec. After cooling on ice for 5 min, 250 μl of LB medium (1% Tryptone, 0.5% Yeast extract and 1% NaCl) was added. After incubated at 310 K for 1 h, the mixture was plated on LB agar (1% Tryptone, 0.5% Yeast extract, 1% NaCl and 1.5% agar) containing 20 μg/ml kanamycin and incubated overnight at 310K. Colonies obtained were used for colony PCR as follows: colonies were selected individually and suspended in 10 μl MilliQ water; 3 μl of the suspension was mixed with 5 μl of Go Taq Green Master Mix (Promega), 1 μg T7 promoter primer and 1 μg S•Tag 18mer primer and used for PCR; 3.5 ml of LB medium containing 20 μg/ml kanamycin was added to the leaving 7 μl suspension and the mixture was incubated at 310 K.

Colony PCR process

Step	Temperature (ºC)	Time (sec)	Cycle
First denaturation	95	120	1
Denaturation	95	30	22
Annealing	52	30	
Extension	72	60	
Last Extension	72	300	1

PCR products were checked by agarose gel electrophoresis. The incubating suspension that succeeded in colony PCR was transferred into 10 ml LB medium and incubated overnight at 310 K. Harvested cells were centrifuged and plasmids were extracted using the Wizard Plus SV Minipreps DNA Purification System (Promega). Finally, the inserted fragments were sequenced by Fasmac DNA Sequence Service.

2.2.2 Transformation and overexpression

The verified pET-47a(+) plasmids were transformed into the expression host *E. coli* Rosetta(DE3) (Novagen). 0.5 μl of CLA-ER/pET47a(+) plasmids and 50 μl of Rosetta(DE3) competent cells were mixed and incubated on ice for 10 min. After heat shock, cooling and incubation as described in 2.2.1, the mixture was plated to LB agar containing 20 μg/ml kanamycin and 34 μg/ml chloramphenicol and incubated overnight at 310 K. Colonies were selected and cultured overnight in 10 ml of LB medium containing 20 μg/ml kanamycin and 34 μg/ml chloramphenicol. The next day, suspension was transferred into 1 L of LB medium and cultured at 310 K until OD_{600} arrived at 0.6. Protein expression was induced by addition of IPTG to a final concentration of 0.5 mM. After cultured for another 16 h at 298 K, the cells were harvested by centrifugation at 5,180 ×g for 10 min and frozen at 193 K.

2.2.3 Purification

Purification of CLA-ER was performed at 4°C. The frozen cells were resuspended in buffer containing 20 mM Tris-HCl (pH 8.0), 300 mM NaCl, 10 mM imidazole, 1 mM DTT, 20 μM NADH and 10 μM FMN, and then disrupted by sonication. After centrifugation at 40,000 ×g for 30 min, the supernatant was applied onto a Ni-NTA superflow (Qiagen) column followed by washing with the same buffer. The fusion protein was cleaved on the column using

HRV3C protease (Novagen) overnight at 277 K. The cleaved protein was eluted with the same buffer and dialyzed against 20 mM Tris-HCl (pH 8.0), 1 mM DTT. As the final step of purification, anion-exchange chromatography was performed with Resource Q 6 ml column (GE Healthcare). The elution fractions were applied to 15% SDS-PAGE to identify the peak and check the purity of CLA-ER. For the stabilization of CLA-ER, 2 mM FMN and 4 mM NADH were added into purified protein. The protein solution was dialyzed against 20 mM Tris-HCl pH 8.0, and then concentrated to 12 mg/ml using Vivaspin 20 (10,000 MWCO) (Sartorius Stedim). The concentration was measured by bicinchoninic acid (BCA) protein assay (46). To confirm the assembly state of purified CLA-ER, size exclusion chromatography was performed at a flow rate of 0.4 ml/min with Superdex 75 HR column (GE Healthcare). The running buffer contained 20 mM Tris-HCl (pH 8.0), 300 mM NaCl and 1 mM DTT.

2.2.4 Crystallization

For the crystallization of CLA-ER with FMN, 2 mM NADH and 4 mM FMN were added to the protein solution. Initial crystallization was performed by the sitting-drop vapor-diffusion method in 96-well intelli-plate (Art Robbins Instruments) using the sparse-matrix screening kits, Crystal Screen HT and Index HT (Hampton Research) at 293 K. Drops containing equal volumes (0.2 μl) of protein solution and crystallization solution were equilibrated against a 40 μl reservoir solution. The plates were sealed with Crystal Clear Sealing Tape (Hampton Research). Crystallization condition was further optimized by 2D grid (pH *vs.* precipitate concentration) at 293 K, with drops containing equal volumes (0.5 μl) of protein solution and crystallization solution.

2.2.5 X-ray data collection and processing

Crystals were picked up with nylon loop (Hampton Research), and then flash-cooled in a stream of cold nitrogen gas without using cryoprotectant. X-ray diffraction data collection was performed at the AR-NE3A beamline at the Photon Factory (Tsukuba, Japan). A dataset of CLA-ER was collected with a wavelength of 1.0000 Å, distance of 244.0 mm between crystal and detector, oscillation range of 0.5º, and exposure time of 1.0 sec per image using an ADSC Quantum 270 CCD detector. 720 images were collected for further processing.

2.2.6 Structure determination, refinement and analysis

The diffraction data were indexed and integrated with XDS, and scaled with XSCALE (47). Upper resolution limit was assessed through the observation of R_{merge}, I/sigma and completeness. The Matthews coefficient or solvent content was estimated to predict the number of molecules in an asymmetric unit. The solvent content of a protein crystal is mostly ranging between 27% and 65% (48). The initial structure of CLA-ER/FMN was determined by molecular replacement (MR) phasing with MOLREP (49). I chose nitroreductase enzyme from *Enterobacter cloacae* (PDB ID 1KQB, sequence identity of 26%) as search model, which also belongs to NADH oxidase/FMN reductase family. The model was iteratively refined using PHENIX (50) and manually refurbished with Coot (51). At the final stage of refinement, water and FMN molecules were added on the basis of f_o - f_c electron density map. The final structure was validated using the RCSB Validation Server (http://deposit.pdb.org/validate/). The Ramachandran plot was validated using Rampage (52). Structural analysis was performed using PyMOL (53). Interactions between CLA-ER and FMN are calculated drawn using LigPlot$^+$ (54).

2.3 Results and discussion

2.3.1 Expression and purification

Amplified CLA-ER gene was confirmed by electrophoresis of PCR product using 1.5% (w/v) agarose. With both colony PCR and DNA sequencing, it was verified that the CLA-ER-coding gene had been inserted into the SmaI/EcoRI site. With plasmids transformed into the expression competent cell *E. coli* Rosetta(DE3), CLA-ER was overexpressed in the soluble fraction. His_6-tagged CLA-ER was purified using Ni-affinity chromatography. Resin showed yellow after CLA-ER solution loaded into the column and washed, which reveals that CLA-ER bound FMN molecules well. Yellow solution eluted from Ni-NTA chromatography was loaded onto the anion-exchange chromatography for further purification (Fig. 2-1). However, the elute fractions were colorless. It indicates that FMN dissociated during anion-exchange chromatography. For the stabilization of CLA-ER, NADH and FMN were added into the CLA-ER solution and the solution showed yellow again. The color retained during the dialysis and concentration, which indicates that CLA-ER bound FMN molecules well. Confirmation of purified CLA-ER sample by SDS-PAGE revealed a single band (Fig. 2-2). Then, assembly state of CLA-ER in solution was investigated by size-exclusion chromatography. Comparison with marker proteins reveals that CLA-ER exists as homodimer in solution (Fig 2-3), which is consistent with other proteins in the NADH oxidase/FMN reductase family.

2.3.2 Crystallization

Initial screening of crystallization was performed using Crystal Screening HT and Index HT. Small crystals in stick shape were obtained in the D10 well of Index HT containing 100 mM

Bis-tris (pH 6.5) and 20% (w/v) PEG monomethyl ether 5,000 after incubation for two days at 293K. The crystallization condition was optimized by the sitting-drop vapor-diffusion method in 96-well plate. A diffraction-quality crystal with a size of 50 × 50 × 200 μm was obtained in the condition of 100 mM Bis-Tris (pH 6.0) and 21% (w/v) PEG monomethyl ether 5,000 (Fig. 2-4).

2.3.3 Data collection and structure determination

The diffraction-quality crystal was used for data collection and a diffraction dataset was collected to an edge of 2.00 Å (Fig. 2-5). The crystal belonged to the primitive triclinic space group *P*1, with unit-cell parameters of a = 49.7, b = 60.9, c = 72.6 Å and α = 85.59, β = 98.92, γ = 111.62º. X-ray diffraction data with resolution up to 2.10 Å were used for structure determination and the data-collection statistics are listed in Table 2-1. The Mathews coefficient and solvent content of the native crystal were estimated to be V_m = 2.10 $Å^3$ Da^{-1} and 41.5%, respectively, which suggested the crystal contained four molecules of CLA-ER in the asymmetric unit. After phasing using molecular replacement, the initial structure of CLA-ER was determined with four molecules per asymmetric unit. By further refinement using PHENIX and coot, the structure of CLA-ER was refined to the final R_{work} and R_{free} of 17.8% and 22.9%, respectively. The parameters for data refinement are listed in Table 2-2 and the final model was shown in Fig. 2-6. Validity of φ and ψ angles were shown in the Ramachandran plot, which indicated that 93.0% of residues in the most favored regions, 6.9% in additional allowed regions and 0.1% in generously allowed regions (Fig. 2-7).

2.3.4 Crystal structure of CLA-ER

The four molecules of CLA-ER in asymmetric unit formed two homodimers that is

consistent with the assembly state in solution (Fig. 2-6). A CLA-ER protomer consists of an α + β fold formed by 9 α-helices and five β-stands with a topology of α1-α2-β1-α3-α4-β2-α5-α6-α7-β3-α8-β4-α9-β5 (Fig. 2-8, 2-9). The structure of CLA-ER is divided into two subdomains, the core subdomain and the flexible subdomain (Fig. 2-9). The core subdomain possesses a central β-sheet that is formed by 4 anti-parallel strands with a fifth β-strand from the C-terminal tail of the other protomer (β5'). The central β-sheet is surrounded by 9 α-helices with a short α-helix on the C-terminal tail of the other protomer (α9') (Fig. 2-9). These observations suggest that the dimeric structure of CLA-ER is stabilized by the domain swapping of the C-terminal tails (Fig. 2-9). In addition, two protomers contact with each other through tight hydrophobic interactions in α7 helices (Fig. 2-10). The flexible subdomains consist of a helix-loop-helix structure (residues 97-132) with a relatively higher *B*-factor (average 47.6 Å) as compared with that of the core subdomain (average 28.7 Å) (Fig. 2-11). In the dimeric structure, two flexible subdomains locate at the both sides of the core subdomain (Fig. 2-9).

2.3.5 FMN recognition of CLA-ER

Two FMN molecules locate within crevices formed at the interface of two core subdomains (Fig. 2-12) and formed extensive interactions with both two protomers (Fig. 2-13 and 2-14). One protomer provides direct hydrogen bonds with FMN and the other one forms hydrophobic interactions and water mediated hydrogen bonds with FMN (Fig. 2-13 and 2-14). Several critical interactions between FMN and CLA-ER are well conserved for enzymatic function. The N1-C2=O2 locus of FMN interacts with Arg24 (Fig. 2-13 and 2-14), which is thought to be relevant to stabilizing the anionic form of the reduced FMN ($FMNH^-$) and increasing the cofactor's redox potential. FMN N5 takes part directly in substrate dehydrogenation and interacts with the backbone of Ser168 on the *si*-face of FMN. This

hydrogen bond is always expected to increase the oxidative power of FMN (55). With the interactions above, the flavins are buried in the surface of the groove mentioned above and orient their *re*-face toward solvent (Fig. 2-12).

Table 2-1 Data-collection statistics of CLA-ER

Source	PF AR-NE3A
Wavelength (Å)	1.0000
Resolution (Å)[a]	20.0–2.10 (2.15–2.10)
Space group	*P*1
Unit cell parameter (Å)	a = 49.7, b = 60.9, c = 72.6,
(°)	α = 85.6, β = 98.9, γ = 111.6
No. observed reflections	176143 (12813)
No. unique reflection	44666 (323)
Average redundancy	3.9 (4.0)
Completeness (%)	97.9 (97.2)
R_{sym}	0.054 (0.315)
Average $\langle I \rangle / \langle \sigma(I) \rangle$	19.6 (4.9)

Values in parentheses are for the highest resolution shell.

[†] $R_{sym} = \Sigma_{hkl} [(\Sigma_i |I_i - \langle I \rangle|) / \Sigma_i |I_i|]$

where I_i is the ith intensity measurement of reflection hkl, including symmetry-related reflections, and $\langle I \rangle$ is its average.

Table 2-2 Data refinement statistics of CLA-ER

R_{work} / R_{free} (%)	17.8/22.9
No. reflections	44650
No. atoms	
Protein	6624
Ligand	124
Water	317
Mean *B* value (Å^2)	
Protein	32.3
Ligand	23.2
Water	32.7
RMSD	
Bond lengths (Å)	0.003
Bond angles (°)	0.831

† $R_{work} = (\Sigma_{hkl} ||F_o| - |F_c||) / \Sigma_{hkl} |F_o|$. 5 % of the data were used for R_{free}.

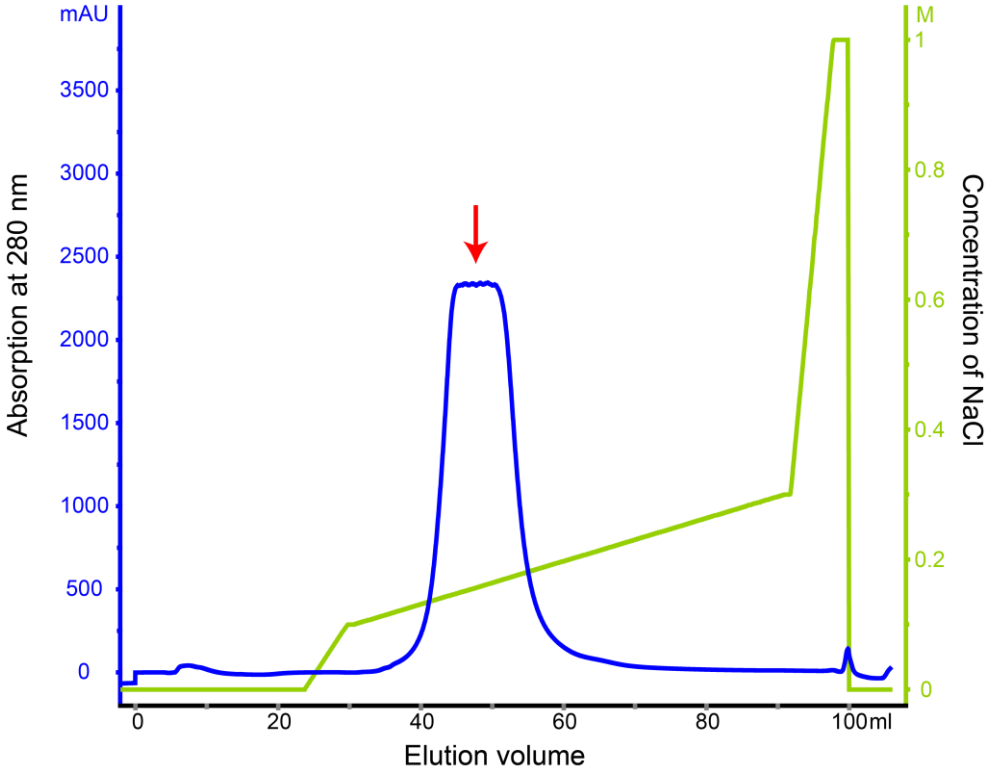

Fig. 2-1 Purification of CLA-ER by anion exchange chromatography. The peak of CLA-ER is indicated by red arrow.

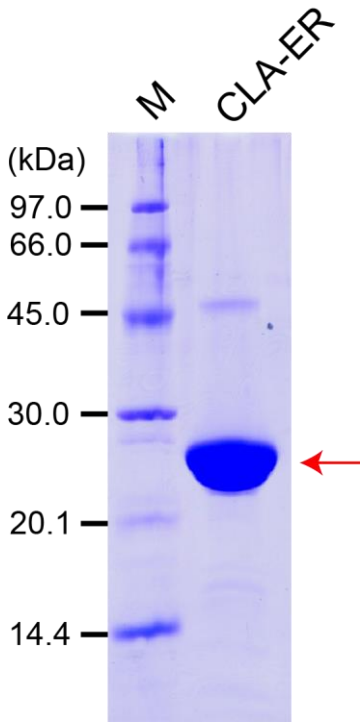

Fig. 2-2 SDS-PAGE of purified sample. The band of CLA-ER is indicated by red arrow.

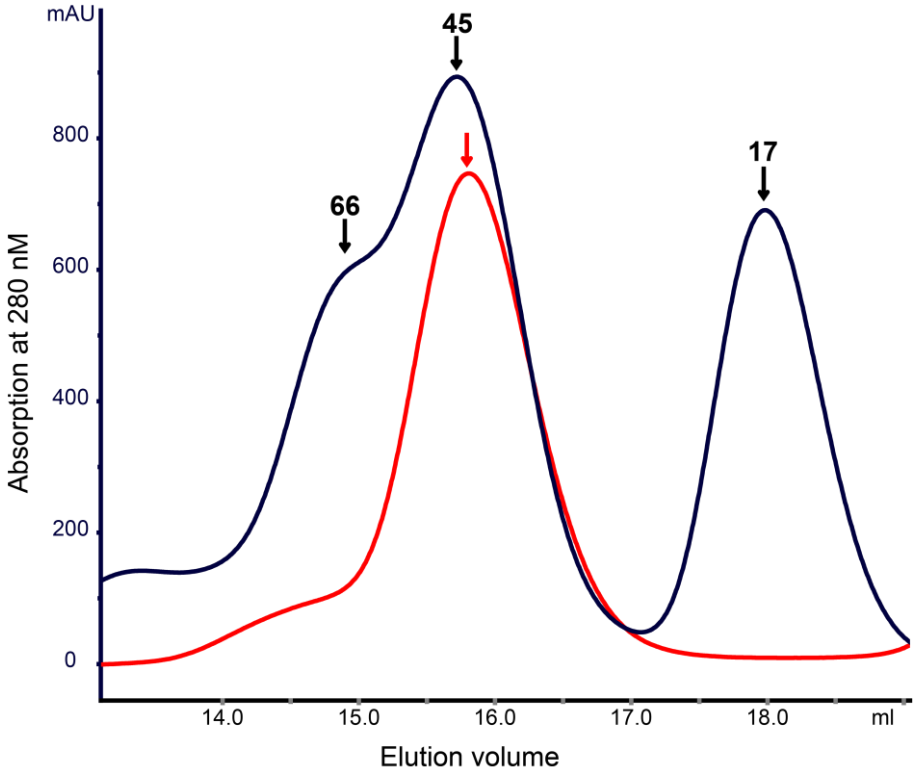

Fig. 2-3 Assembly state analysis of CLA-ER by size-exclusion chromatography. The molecule-masses of markers are labeled above the peaks (kDa). The peak of CLA-ER is indicated by red arrow.

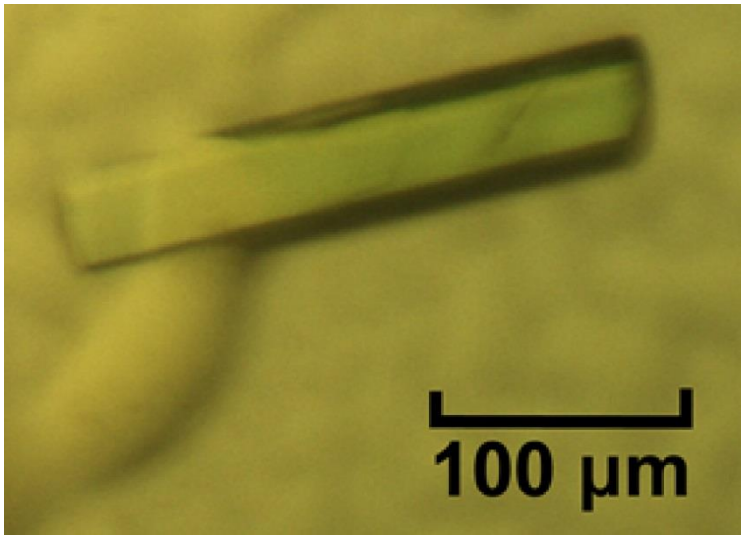

Fig. 2-4 Diffraction-quality crystal of CLA-ER crystallized in the solution containing 0.1 M Bis-Tris (pH 6.0) and 21% (w/v) PEG monomethyl ether 5,000 at 293 K.

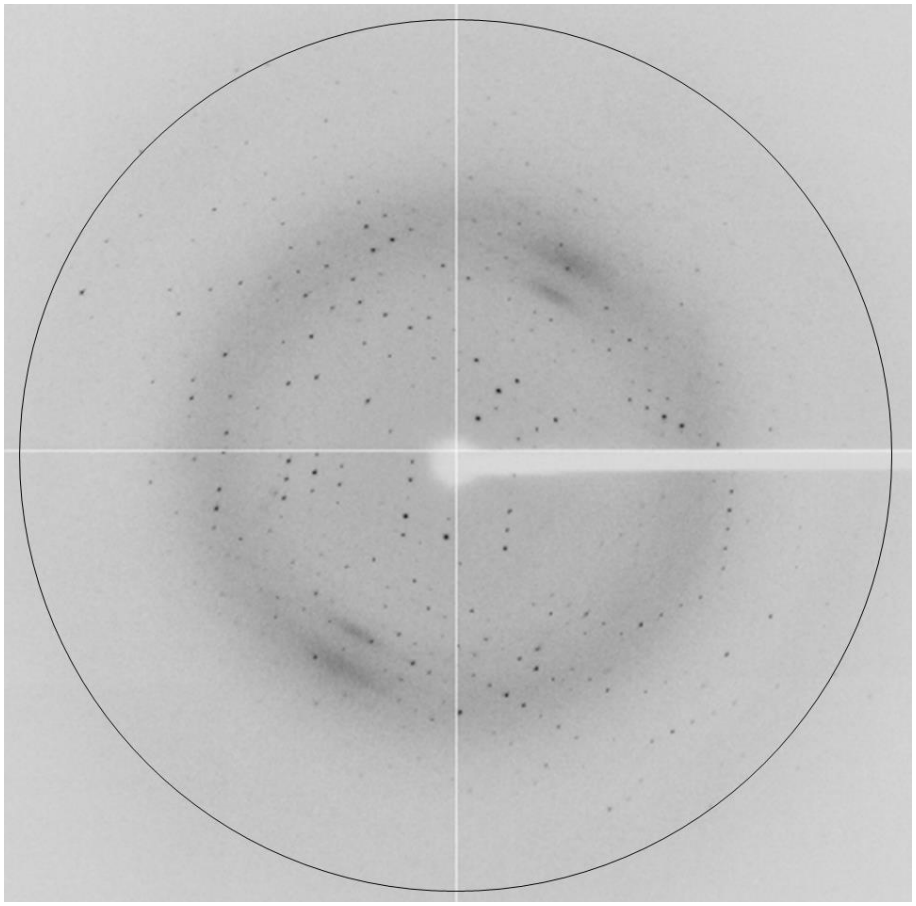

Fig 2-5 An X-ray diffraction image collected from a crystal of CLA-ER. A resolution limit of 2.10 Å is indicated by black circle.

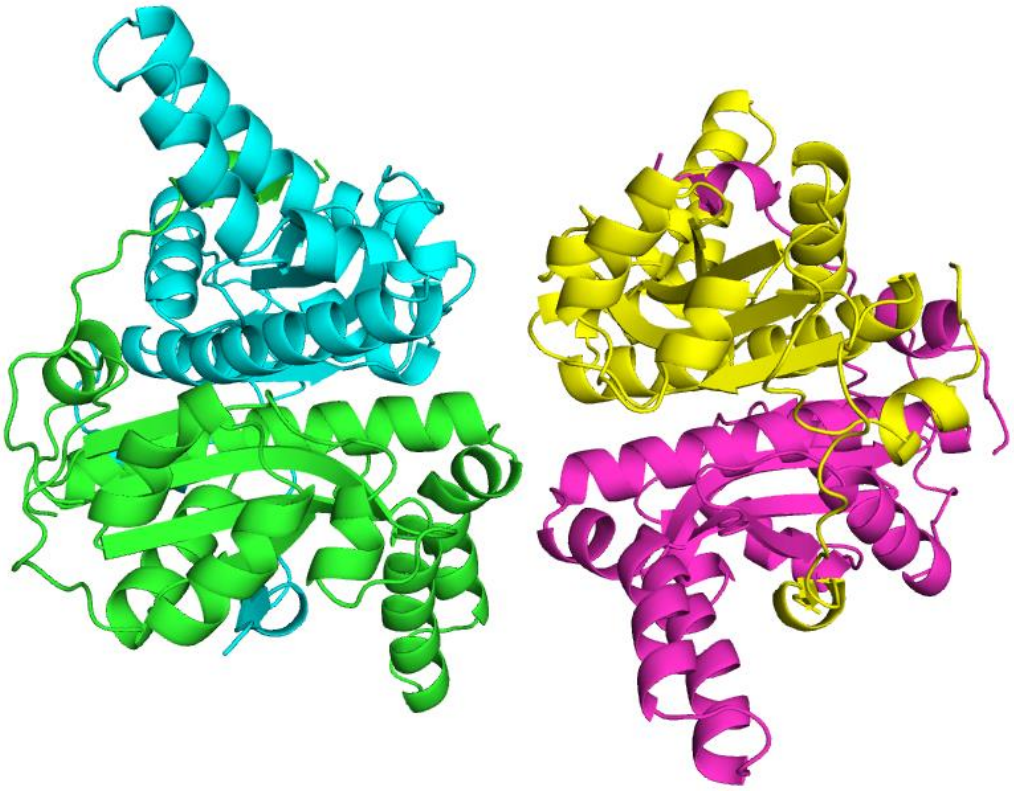

Figure 2-6 Final model of CLA-ER structure with four molecules in an asymmetric unit. Each molecule is colored differently.

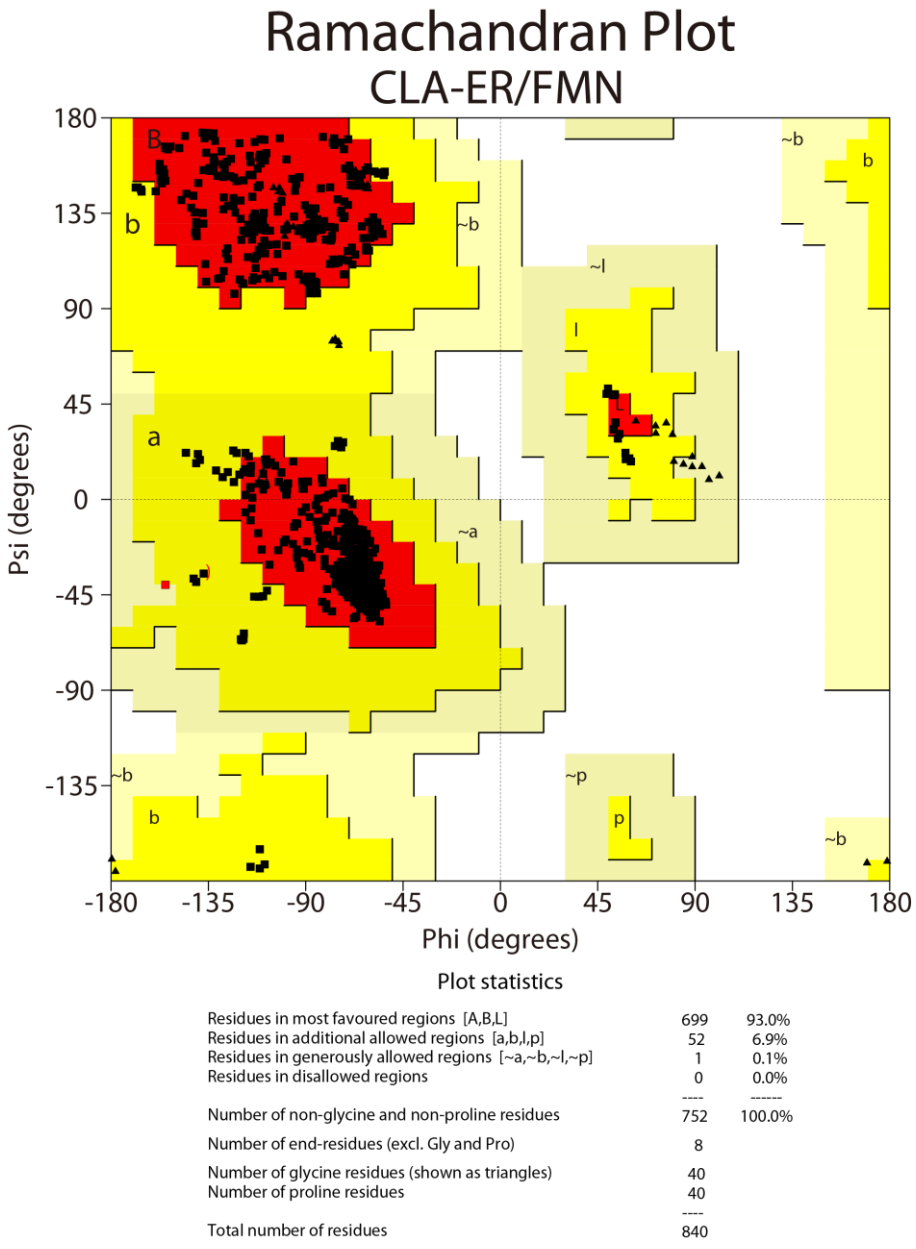

Fig. 2-7 Ramachandran plot of CLA-ER. The percentage of the residues in the most favored regions, additional allowed regions and generously allowed regions are 93.0%, 6.9% and 0.1%, respectively.

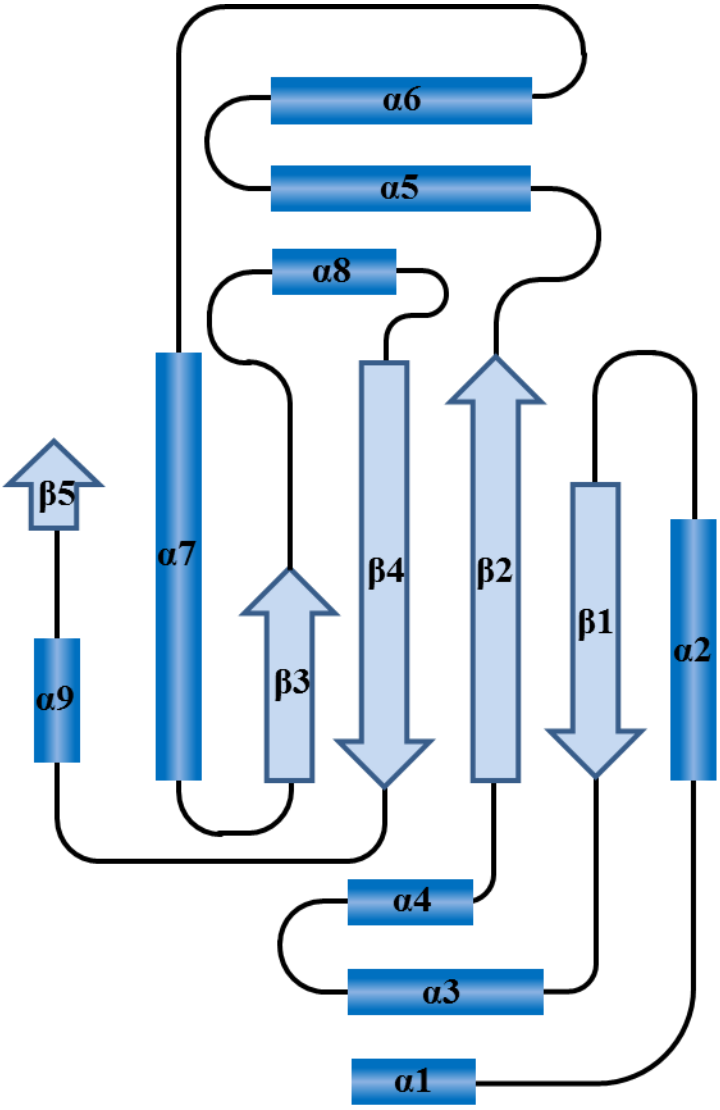

Fig 2-8 Diagram of CLA-ER topology. α-helices and β-strands are indicates as cylinders and arrows, respectively.

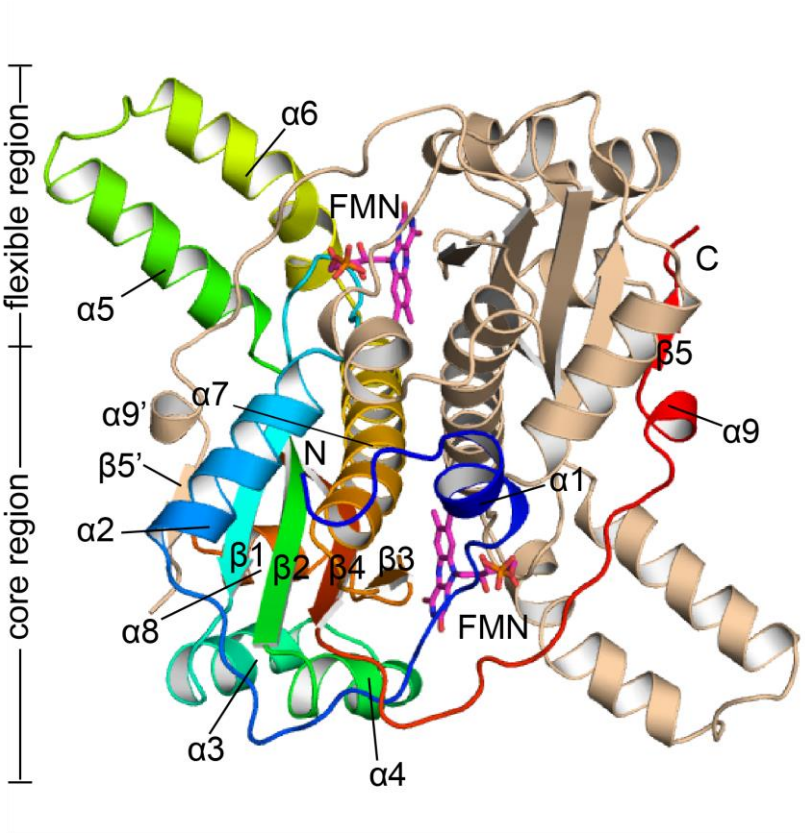

Figure 2-9 Dimer structure of CLA-ER. One protomer is shown in rainbow color from the N-terminus (violet) to C-terminus (red) and the other is colored wheat. FMN molecules are highlight as stick model in yellow.

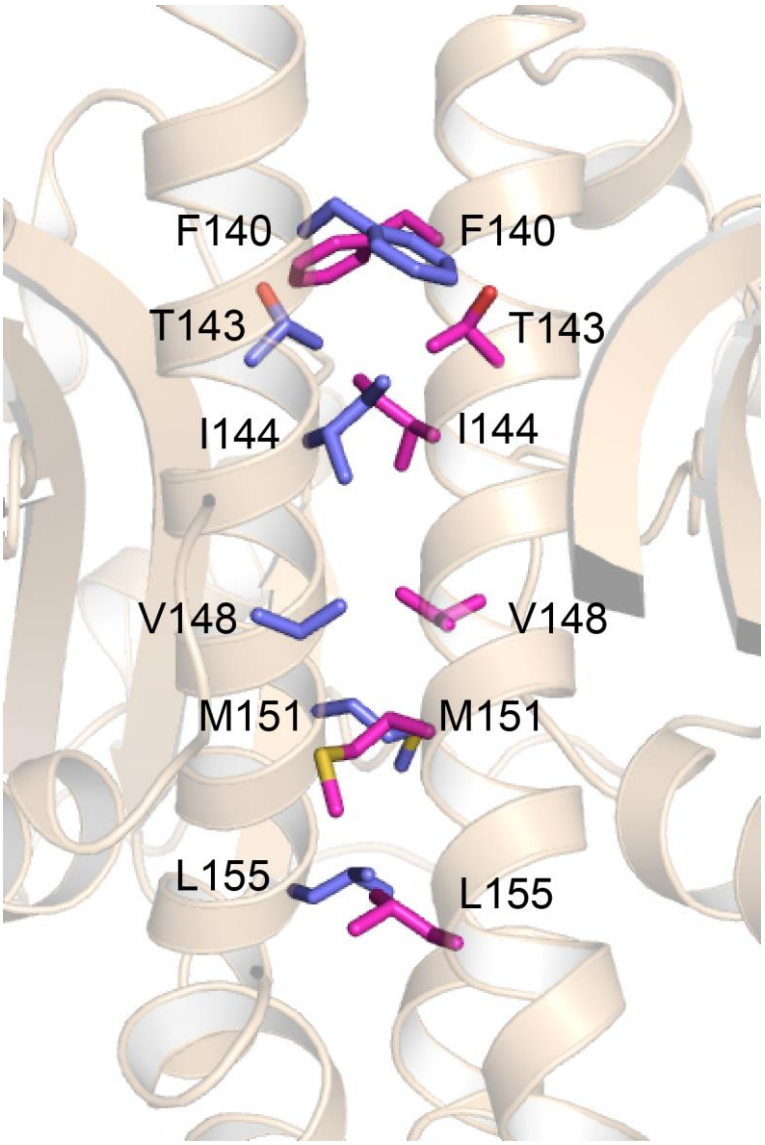

Fig 2-10 Hydrophobic interactions in α7 helices.

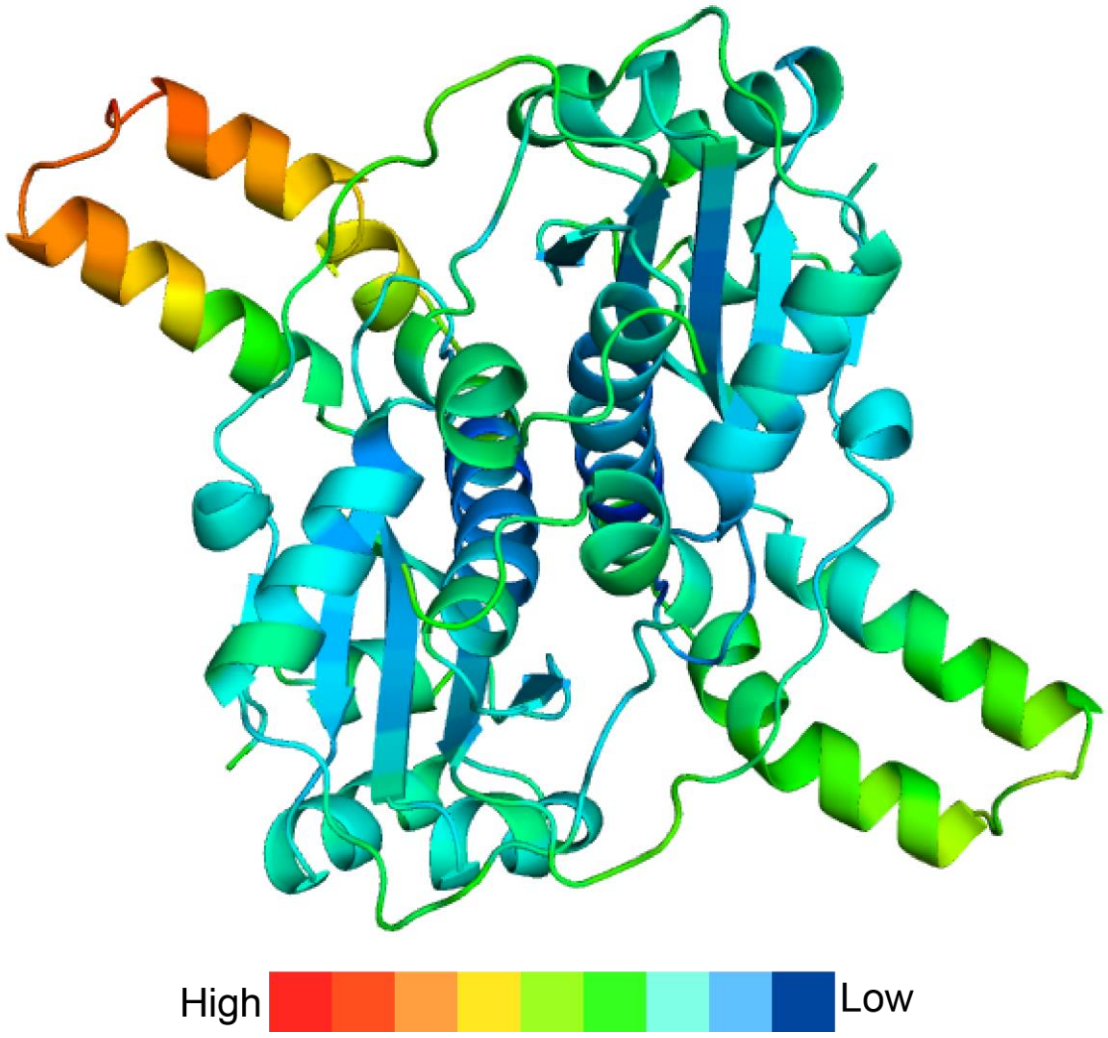

Fig. 2-11. Crystal structure of CLA-ER colored by *B* factor from blue (low) to red (high)

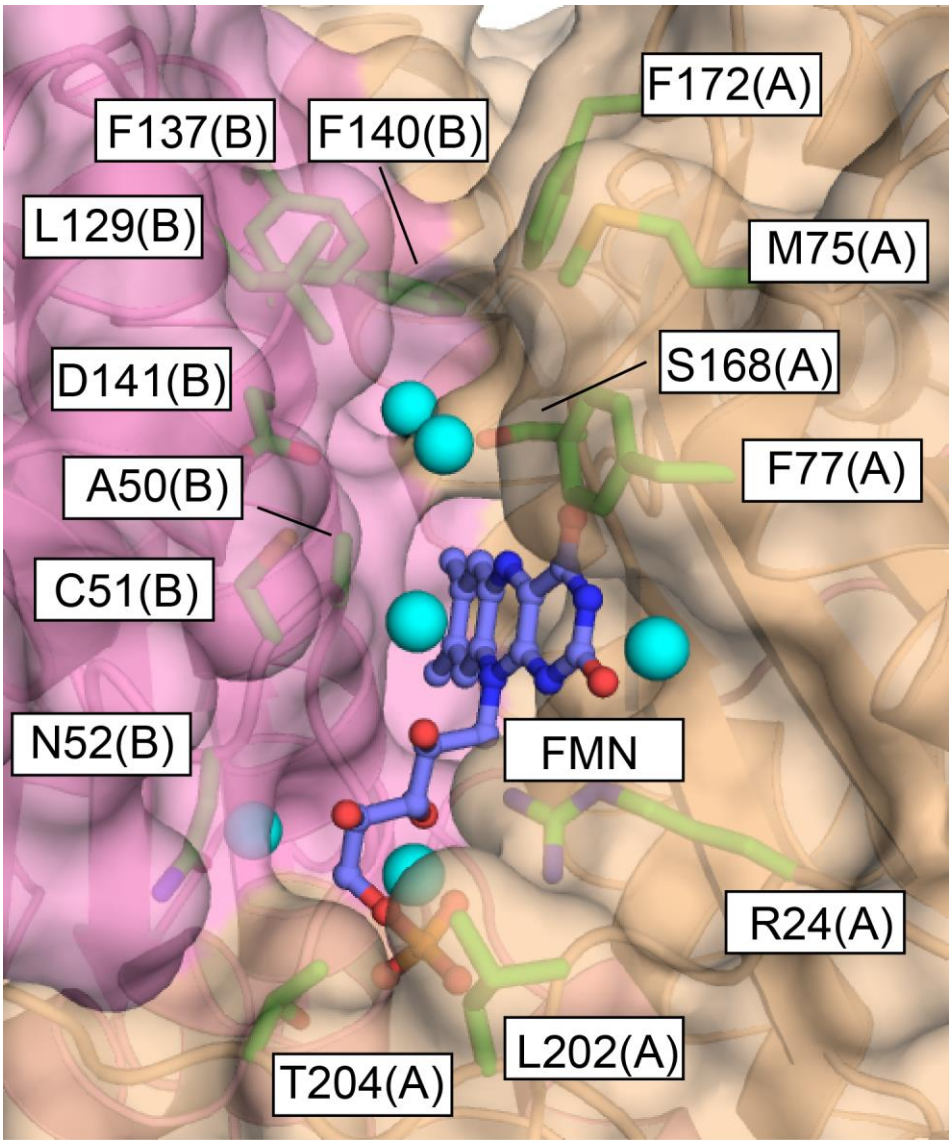

Fig 2-12 Groove for FMN binding. Water and FMN molecules are indicated by cyan sphere and slate stick-ball model, respectively.

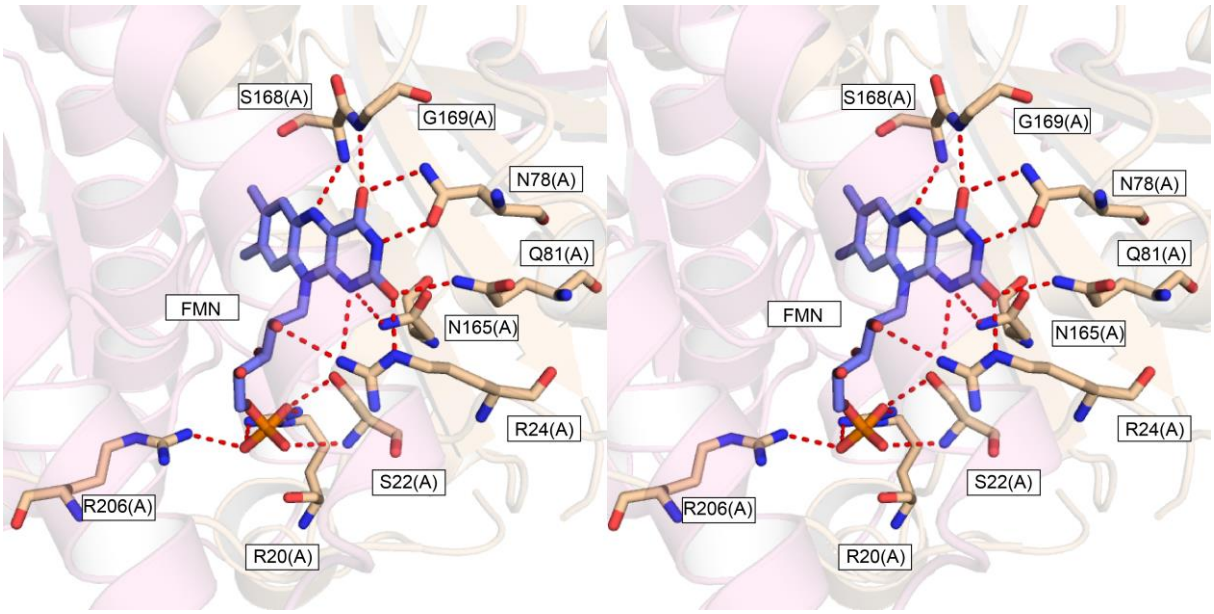

Fig. 2-13 Stereo view of hydrophilic interactions between CLA-ER and FMN.

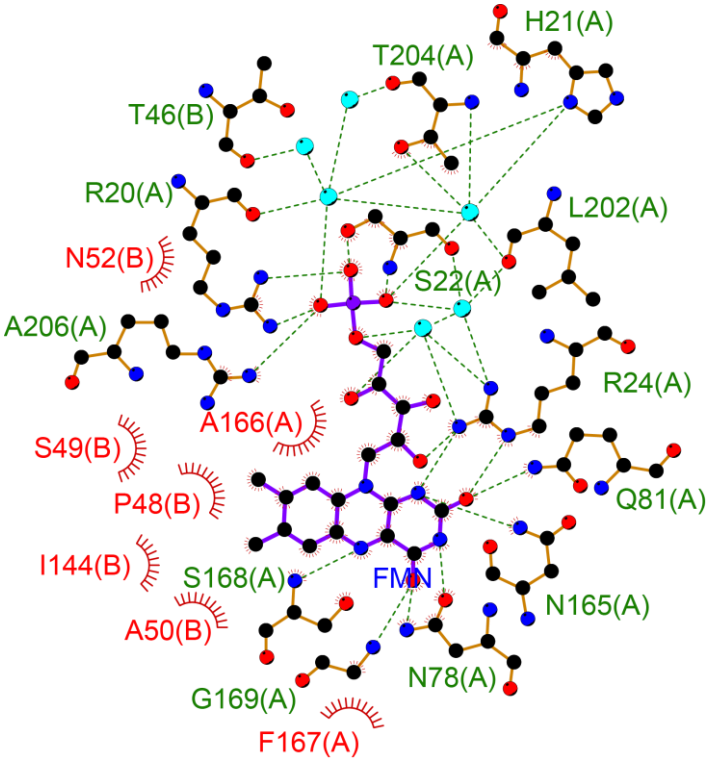

Fig 2-14 Schematic representation for non-covalent interactions between CLA-ER and FMN. Hydrogen bonds and hydrophobic interactions are indicated by green dashed line and red arc, respectively.

Chapter 3

X-ray Structural Analysis of CLA-ER/FMN/KetoB and CLA-ER/FMN/KetoC

3.1 Exordium

Crystal structure of CLA-ER in the presence of FMN has been described in Chapter 2, which revealed not only the structural features of CLA-ER but also the recognition mechanism of cofactor FMN. However, it remains unclear how CLA-ER recognize its substrate. In order to elucidate ligand recognition mechanism, co-crystallization is usually performed in the presence of ligand or its analogs. In this chapter, I will describe protein preparation, co-crystallization, structure determination and analysis of CLA-ER in the presence of KetoB or KetoC.

3.2 Materials and Methods

3.2.1 Preparation for co-crystallization

Purification of CLA-ER was performed in the same manner as described in Chapter 2. The CLA-ER was overexpressed in Rosetta(DE3), purified by Ni-NTA superflow chromatography and anion exchange chromatography, and stabilized by the addition of excess NADH and FMN cofactors. After dialysis and concentration, the concentration of purified protein was measured by BCA.

3.2.2 Crystallization

For co-crystallization, KetoB and KetoC were added into prepared CLA-ER solution (12 mg/ml) to a final concentration of 2 mM and the mixtures were incubated overnight at 4ºC. The precipitate was filtered after incubation and supernatant was used for co-crystallization. Initial crystallization was performed by the sitting-drop vapor-diffusion method in 96-well intelli-plate using the sparse-matrix screening kits, Crystal Screen HT, Index HT and EasyXtal JCSG+ Suite (Qiagen) at 293 K. Optimization of crystallization condition is performed as described in Chapter 2.

3.2.3 X-ray data collection and processing

Each crystal was picked up with nylon loop and frozen in a stream of cold nitrogen gas stream without using cryopretectant. X-ray diffraction experiments were performed at the AR-NE3A beamline at the Photon Factory. A dataset of CLA-ER with KetoB was collected with a wavelength of 1.0000 Å, distance of 240.0 mm between crystal and the detector,

oscillation range of 0.5º, and exposure time of 1.0 sec per image using an ADSC Quantum 270 CCD detector. 360 images were collected for further processing. For CLA-ER with KetoC, similar X-ray diffraction experiments were performed. A dataset was collected in the same condition as CLA-ER with KetoB.

3.2.4 Structure determination, refinement and structural analysis

The diffraction data were indexed and integrated with XDS, and scaled with XSCALE. The initial structures of CLA-ER/FMN/KetoB and CLA-ER/FMN/KetoC were determined by molecular replacement phasing with MOLREP using CLA-ER/FMN as search model. After refinement using PHENIX, the model was rebuilt using ARP/wARP (56). The new model was iteratively refined using PHENIX and manually refurbished with Coot. At the final stage of refinement, FMN, KetoB/KetoC and water molecules were added on the basis of f_o - f_c electron density map. The final structure was validated using the RCSB Validation Server. The Ramachandran plot was validated using Rampage. Structural analysis and electrostatic surface potential calculation were performed using PyMOL. Interactions between CLA-ER and KetoC are calculated and drawn using LigPlot$^+$.

3.2.5 Size exclusion chromatography

To confirm the assembly state of purified CLA-ER in fatty acid-bound state, solution prepared for co-crystallization was loaded into a Superdex 75 HR column. Size exclusion chromatography was performed at a flow rate of 0.4 ml/min with Superdex 75 HR column. The running buffer contained 20 mM Tris-HCl (pH 8.0), 300 mM NaCl and 1 mM DTT.

3.3 Results and discussion

3.3.1 Co-crystallization

Initial screening of crystallization was performed using Crystal screening HT, Index HT and EasyXtal JCSG+ Suite. Crystals of CLA-ER with KetoB or KetoC were obtained in various conditions. After optimization of these conditions, diffraction-quality crystals for CLA-ER/FMN/KetoB were obtained in the condition of 100 mM Tris-HCl (pH 9.0) and 2.0 M ammonium sulfate (Fig. 3-1 A). Diffraction-quality crystals for CLA-ER/FMN/KetoC were obtained in the condition of 100 mM sodium cacodylate (pH 6.8), 200 mM NaCl and 2.0 M ammonium sulfate (Fig. 3-1 B). The shapes of these crystals were different from that of CLA-ER/FMN.

3.3.2 Data collection and structure determination

The crystals were used for data collection. A diffraction dataset of CLA-ER/FMN/KetoB was collected to an edge of 2.00 Å (Fig. 3-2 A). The crystal belonged to the centered orthorhombic space group $C222_1$, with unit-cell parameters of a = 65.0, b = 68.9, c = 197.6 Å. X-ray diffraction data with resolution up to 2.35 Å were used for structure determination and the data-collection statistics are listed in Table 3-1. The Mathews coefficient and solvent content of the crystal were estimated to be V_m = 2.27 $Å^3$ Da^{-1} and 45.9%, respectively, which suggested the crystal contained two molecules of CLA-ER in the asymmetric unit. After phasing using molecular replacement, the initial structure of CLA-ER/FMN/KetoB was determined with two molecules per asymmetric unit. By further refinement using PHENIX, ARP/wARP and coot, the structure of CLA-ER was refined to final R_{work} and R_{free} of 18.6% and 23.9%, respectively. The parameters for data refinement are listed in Table 3-2. The final model was shown in Fig. 3-3. Validity of φ and ψ were shown in the Ramachandran plot,

which indicated that 91.6% of residues in the most favored regions, 8.4% in additional allowed regions (Fig. 3-4).

A diffraction dataset of CLA-ER/FMN/KetoC was also collected to an edge of 2.00 Å (Fig. 3-2 B). The crystal belonged to the centered orthorhombic space group $C222_1$, with unit-cell parameters of a = 65.0, b = 68.9, c = 197.6 Å. X-ray diffraction data with resolution up to 2.15 Å were used for structure determination and the data-collection statistics are listed in Table 3-1. After phasing using molecular replacement, the initial structure of CLA-ER/FMN/KetoC was determined with two molecules per asymmetric unit. By further refinement using PHENIX, ARP/wARP and coot, the structure of CLA-ER was refined to final working R and free R factors of 19.1% and 23.8%, respectively. The parameters for data refinement are listed in Table 3-2. Validity of φ and ψ were shown in the Ramachandran plot, which indicated that 93.7% of residues in the most favored regions, 6.3% in additional allowed regions (Fig. 3-5).

3.3.3 Crystal structures of CLA-ER/FMN/KetoB and CLA-ER/FMN/KetoC

Crystal structures of CLA-ER/FMN/KetoB and CLA-ER/FMN/KetoC were superimposed with an RMSD of 0.141 Å (Fig. 3-6), which indicates that the two structures shared a similar structure. Therefore, I used the structure of CLA-ER/FMN/KetoC for further discussion due to its relatively high resolution.

KetoC-bound CLA-ER showed a similar structure to fatty acid-free CLA-ER, except for the orientation of the flexible subdomain. According to the electron density, the C-terminal tails extended away from core subdomain and interacted with the adjacent CLA-ER homodimers in the same manner (Fig. 3-7).

3.3.4 Assembly state of CLA-ER in KetoC-bound state

Size exclusion chromatography was performed to investigate the assembly state of KetoC-bound CLA-ER. The result showed that CLA-ER also formed dimer in the KetoC-bound state and the molecular size is more compact that that in fatty acid-free state (Fig. 3-8). It indicates that the extension of C-terminal tails is due to the condition of crystallization.

3.3.5 Structure remodeling

It has been demonstrated that KetoC-bound CLA-ER keeps its homodimeric conformation in solution. Superimposition of the core subdomains of CLA-ER in KetoC-bound state and fatty acid-free state revealed a similar structure and spatial arrangement of C-terminal tails (Fig. 3-9). Considering its dimeric state in solution, I remodeled the C-terminal tail structures of CLA-ER/FMN/KetoC according to those in fatty acid-free state (Fig. 3-10). The *B*-factor of CLA-ER/FMN/KetoC is lower than that of CLA-ER/FMN, especially in the flexible subdomain (Fig. 2-11, Fig. 3-11). It indicates that the binding of KetoC contribute to the stabilization of CLA-ER.

3.3.5 KetoC recognition by CLA-ER

The electron density of KetoC was observed near FMN. The electron density is clear in enoate group, but not clear in two ends (Fig. 3-12). . To clarify the orientation of KTC, both models of KTC with reversed orientations were built according to the electron density (Fig. 3-13). The KTC model with carboxy group oriented in P200 was fit with the shape of the binding site. However, the opposite KTC model collided with the wall. These observations conclude that CLA-ER bind KTC with carboxy group oriented in P200.

The residues around KetoC also come from two protomers as those for FMN recognition (Fig. 3-14), which indicates that the dimeric structure of CLA-ER is essential for the recognition of substrate and reaction. These residues form a tunnel in a long sandglass shape that is narrow in the middle and relatively wide in two ends (Fig. 3-15). C51, F126 and the flavin ring of FMN locate at the middle region of the tunnel with a suitable space for the enoate group of fatty acid (Fig. 3-15). All the basic residues involved in the formation of the tunnel locate in the carboxyl group side and the hydrophobic residues were observed in the alkyl group side (Fig. 3-14), which results in a basic half and a hydrophobic half of tunnel (Fig. 3-15). Further analysis of interactions between CLA-ER and KetoC reveals that KetoC mainly forms hydrophobic interactions with CLA-ER, involving residues of A50, C51, W105, R118, I122, F126, L129, Y130, F137 from one protomer and R24, F77, S168 from the other (Fig. 3-16). The sole hydrophilic interaction is observed between the carbonyl group of KetoC and amino group of C51 (Fig. 3-16). Both the sandglass shape of the tunnel and the lack of hydrogen bonds lead to diverse forms of KetoC, which is the reason of a strong electron density in the carbonyl group of KetoC and a weak electron density in both the two ends (Fig. 3-12).

Table 3-1 Data-collection statistics of CLA-ER with fatty acids binding

	CLA-ER/FMN/KetoB	CLA-ER/FMN/KetoC
Source	PF AR-NE3A	PF AR-NE3A
Wavelength (Å)	1.0000	1.0000
Resolution (Å)[a]	20.0–2.35 (2.41–2.35)	20.0–2.15 (2.21–2.15)
Space group	$C222_1$	$C222_1$
Unit cell parameter (Å)	a = 65.3, b = 68.4, c = 197.8	a = 65.0, b = 68.9, c = 197.6
No. observed reflections	134192 (9955)	174624 (12852)
No. unique reflection	18830 (1345)	24490 (1735)
Average redundancy	7.1 (7.4)	7.1 (7.4)
Completeness (%)	99.8 (100)	99.8 (100)
R_{sym}	0.099 (0.411)	0.010 (0.392)
Average $<I>/<\sigma(I)>$	16.1 (5.3)	15.1 (5.3)

Values in parentheses are for the highest resolution shell.

[†] $R_{sym} = \Sigma_{hkl} [(\Sigma_i |I_i - \langle I \rangle|) / \Sigma_i |I_i|]$

where I_i is the ith intensity measurement of reflection hkl, including symmetry-related reflections, and $\langle I \rangle$ is its average.

Table 2-2 Data refinement statistics of CLA-ER

	CLA-ER/FMN/KetoB	CLA-ER/FMN/KetoC
R_{work} / R_{free} (%)	18.6/23.9	19.1/23.8
No. reflections	18823	24481
No. atoms		
Protein	3363	3363
Ligand	104	104
Water	124	225
Mean *B* value (Å^2)		
Protein	30.2	25.25
Ligand	27.4	22.9
Water	28.8	27.8
R.m.s.deviations		
Bond lengths (Å)	0.003	0.004
Bond angles (°)	0.832	0.904

† $R_{factor} = (\Sigma_{hkl} ||F_o| - |F_c||) / \Sigma_{hkl} |F_o|$. 5 % of the data were used for R_{free}.

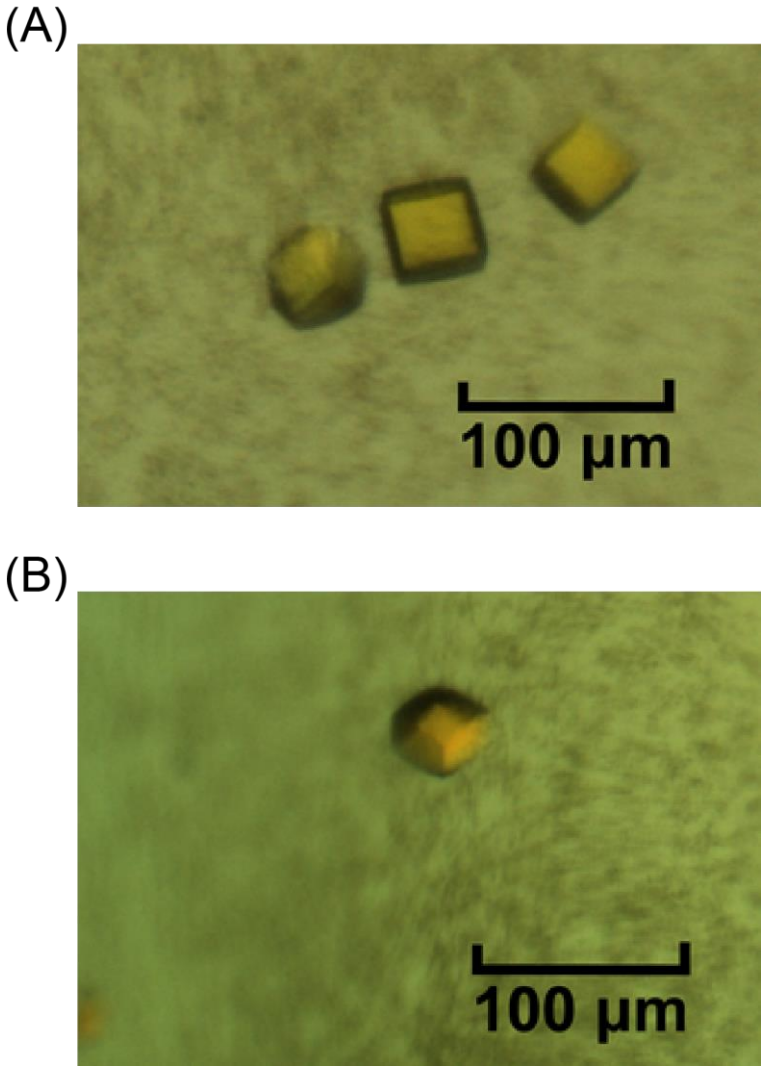

Fig. 3-1 Diffraction-quality crystal of CLA-ER in fatty acid-bound state. (A) Crystals of CLA-ER/FMN/KetoB obtained in the condition of 100 mM Tris-HCl (pH 9.0) and 2.0 M ammonium sulfate. (B) Crystal of CLA-ER/FMN/KetoC obtained in the condition of 100 mM sodium cacodylate (pH 6.8), 200 mM NaCl and 2.0 M ammonium sulfate.

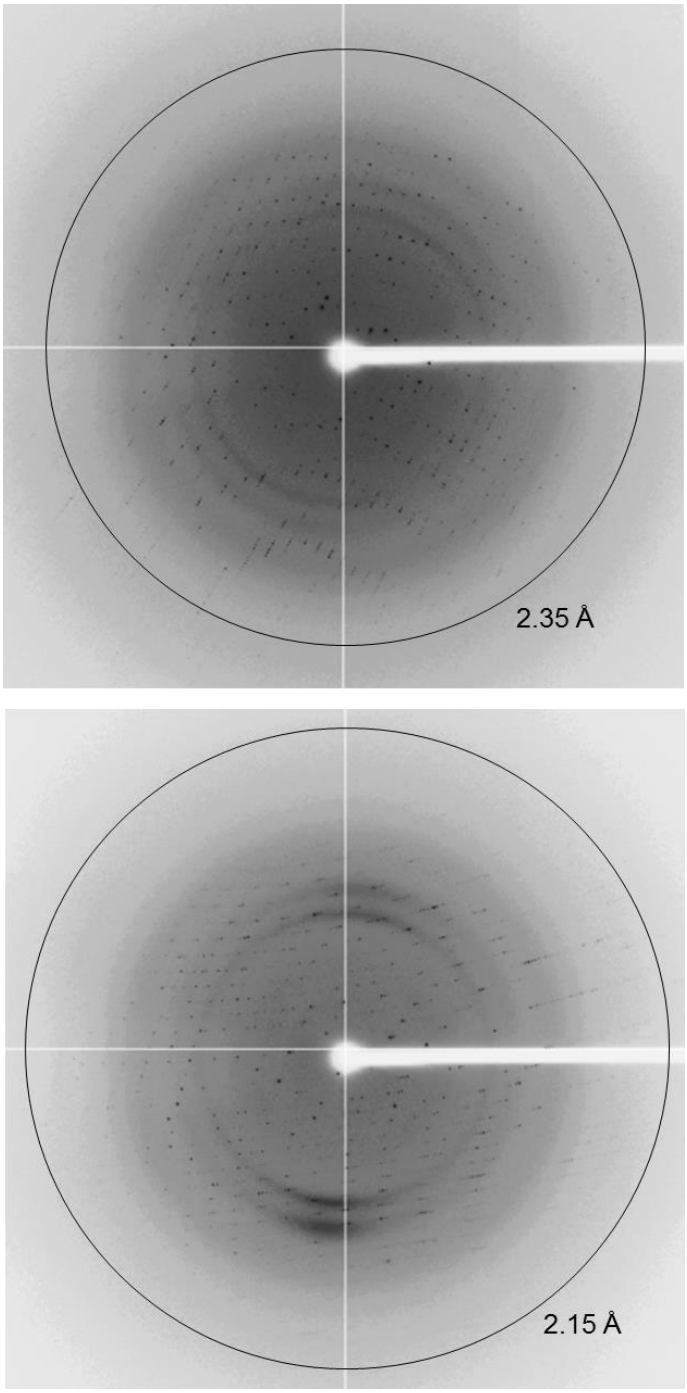

Fig. 3-2 X-ray diffraction images collected from crystals of CLA-ER/FMN/KetoB and CLA-ER/FMN/KetoC. Resolution limits used for structure determination are indicated by black circle. (A) Diffraction image of CLA-ER/FMN/KetoB. (B) Diffraction image of CLA-ER/FMN/KetoC.

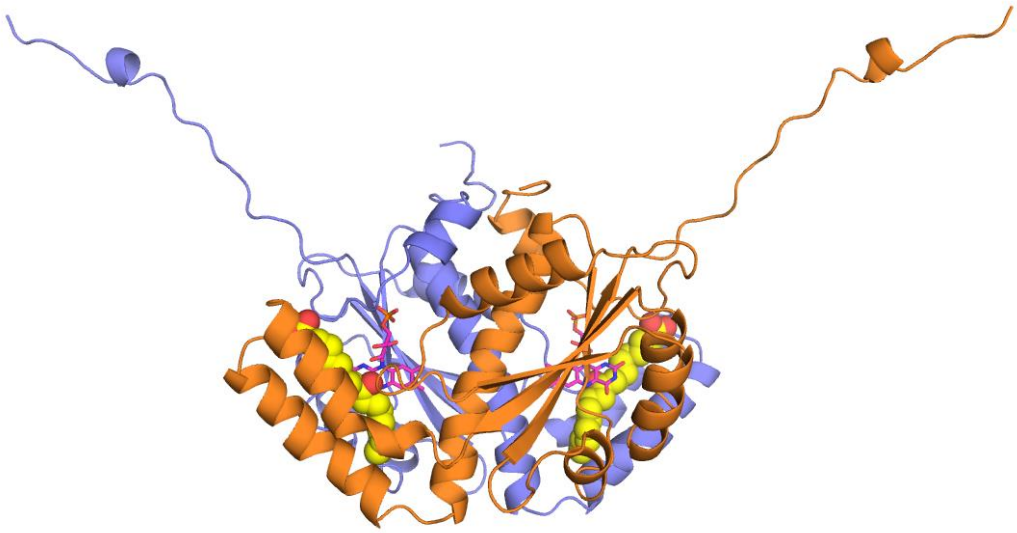

Fig. 3-3 Two molecules of CLA-ER in the presence of FMN and fatty acid in an asymmetric unit. Each molecule is colored differently. FMN and fatty acid molecules are indicated by magenta stick and yellow sphere, respectively.

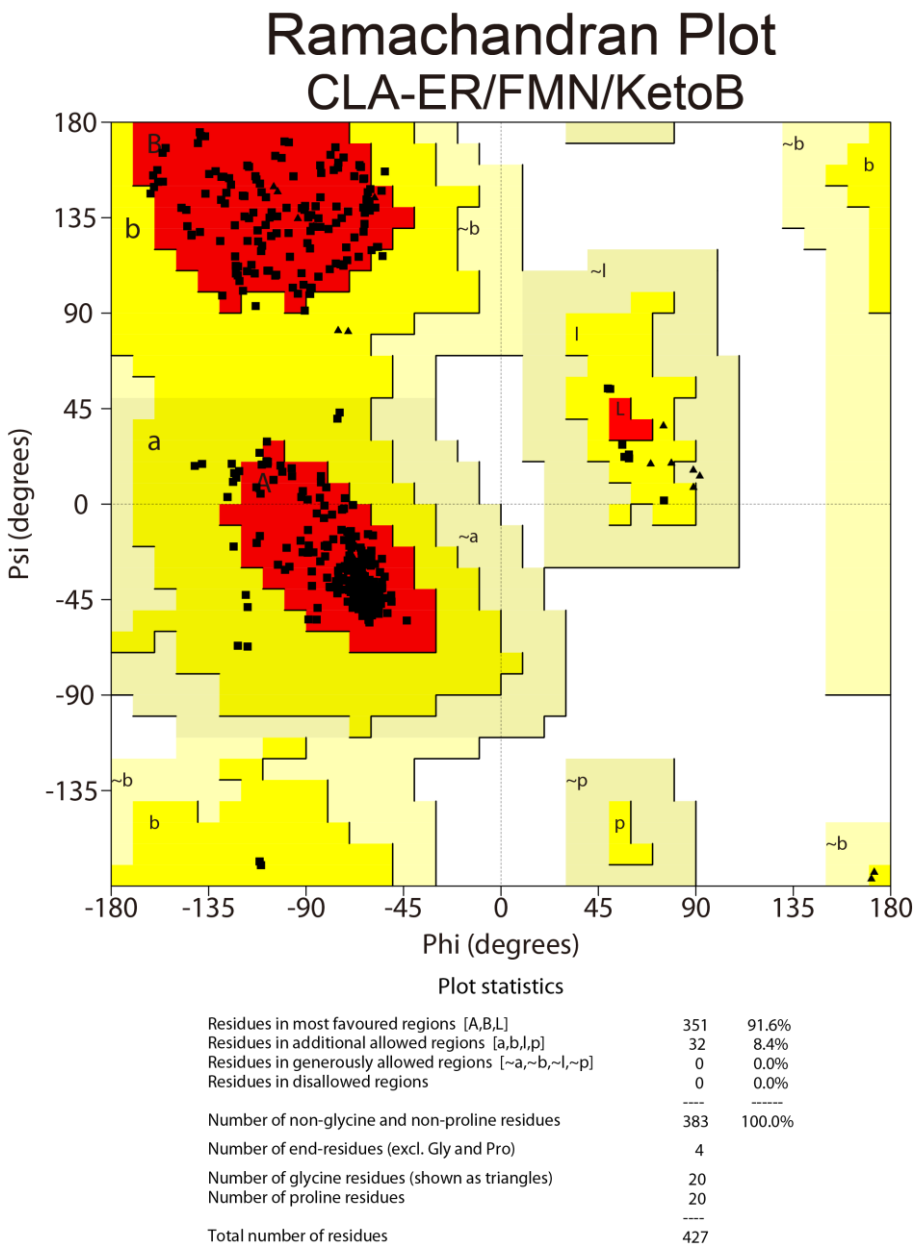

Fig. 3-4 Ramachandran plot of CLA-ER/FMN/KetoB. The percentage of the residues in the most favored regions and additional allowed regions are 91.6% and 8.4%, respectively.

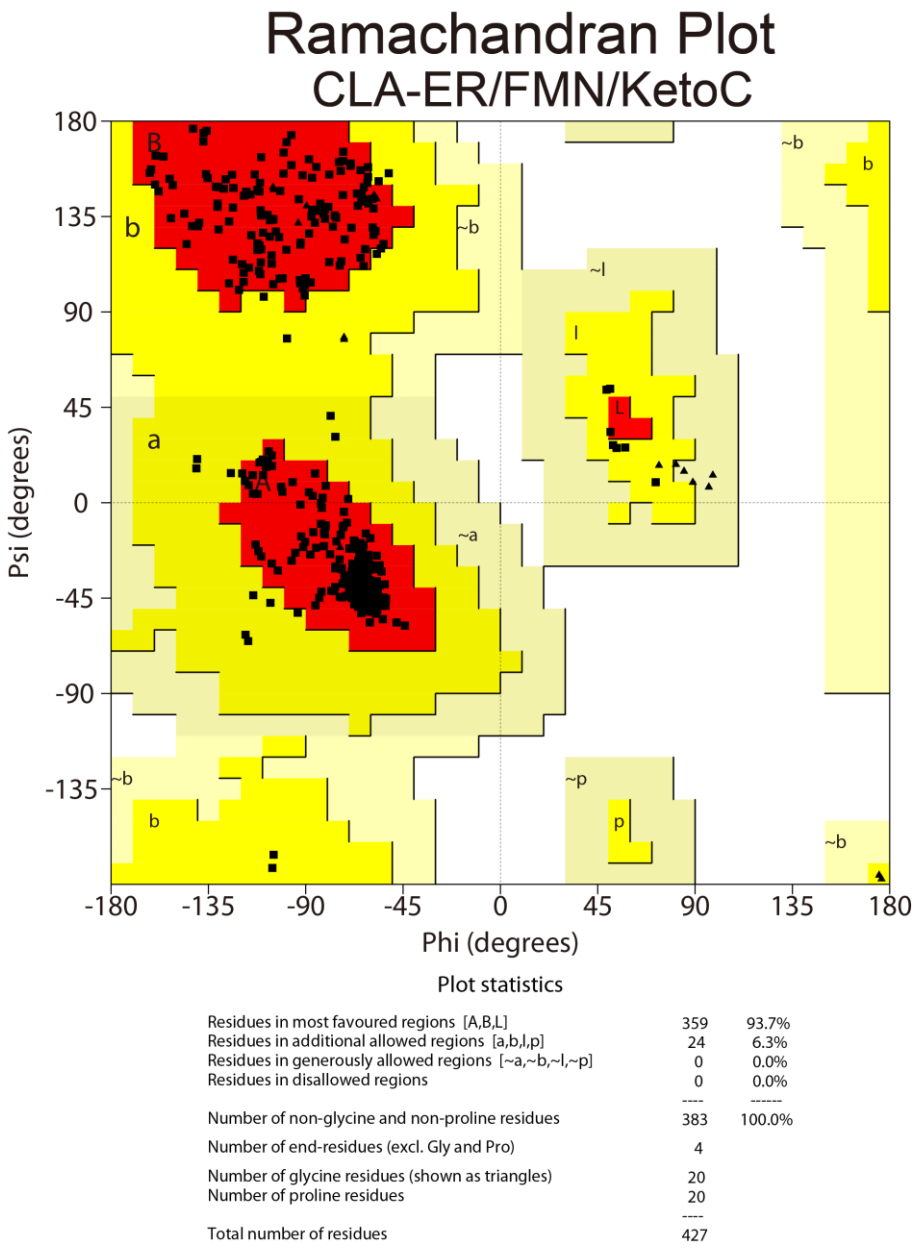

Plot statistics

Residues in most favoured regions [A,B,L]	359	93.7%
Residues in additional allowed regions [a,b,l,p]	24	6.3%
Residues in generously allowed regions [~a,~b,~l,~p]	0	0.0%
Residues in disallowed regions	0	0.0%
Number of non-glycine and non-proline residues	383	100.0%
Number of end-residues (excl. Gly and Pro)	4	
Number of glycine residues (shown as triangles)	20	
Number of proline residues	20	
Total number of residues	427	

Fig. 3-5 Ramachandran plot of CLA-ER/FMN/KetoB. The percentage of the residues in the most favored regions and additional allowed regions are 93.7% and 6.3%, respectively.

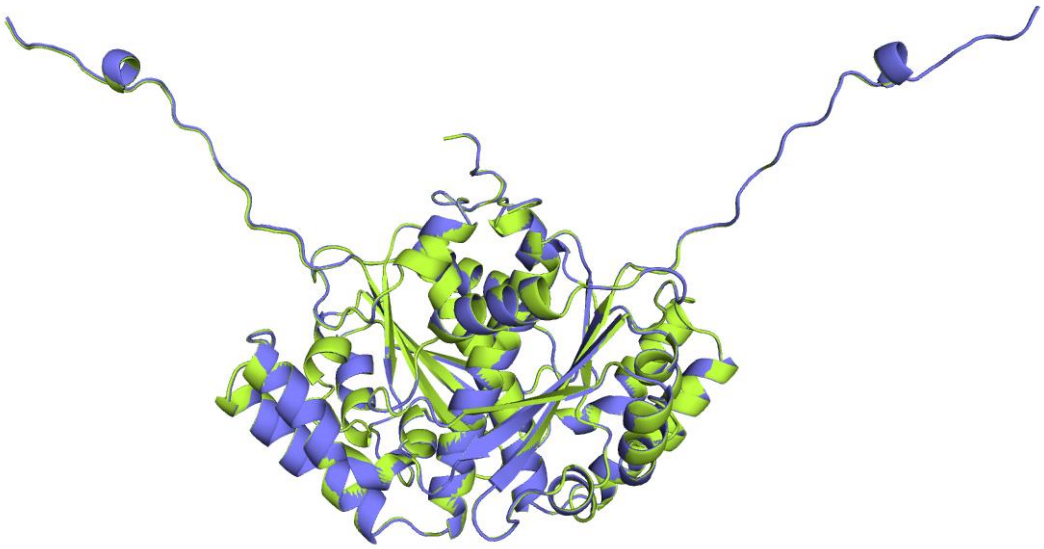

Fig. 3-6 Superimposition of CLA-ER/FMN/KetoB (slate) and CLA-ER/FMN/KetoC (limon).

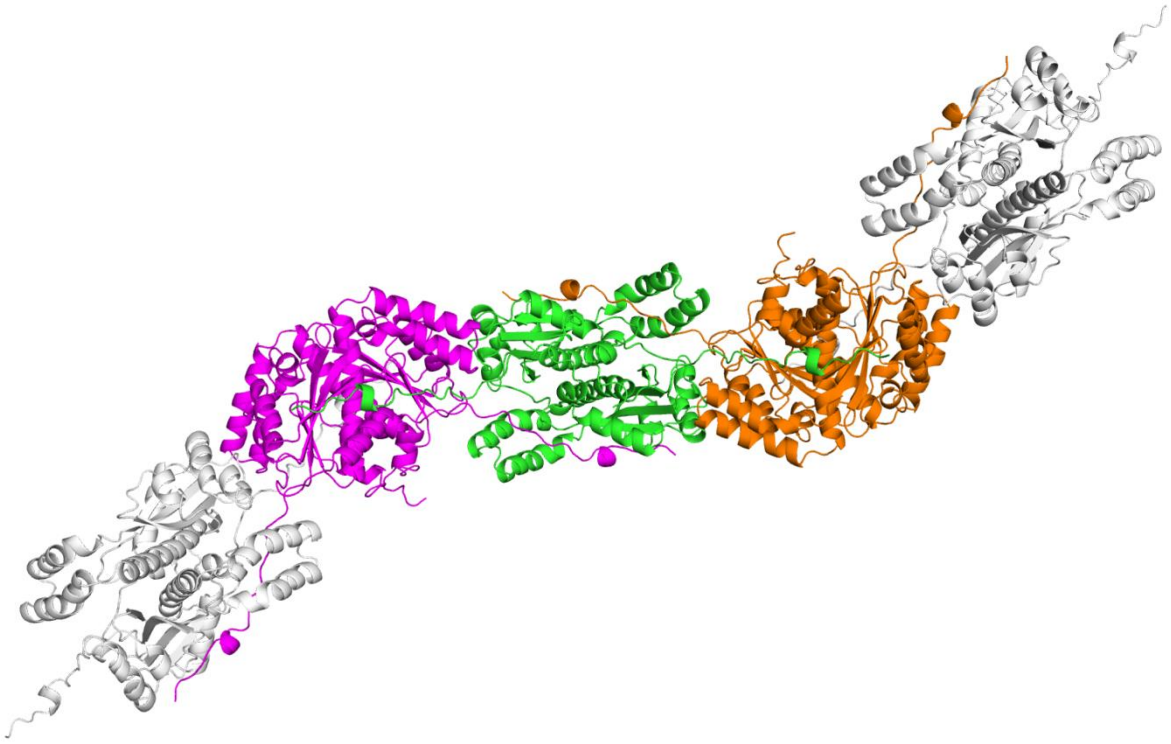

Fig. 3-7 Packing of CLA-ER/FMN/KetoC in crystal.

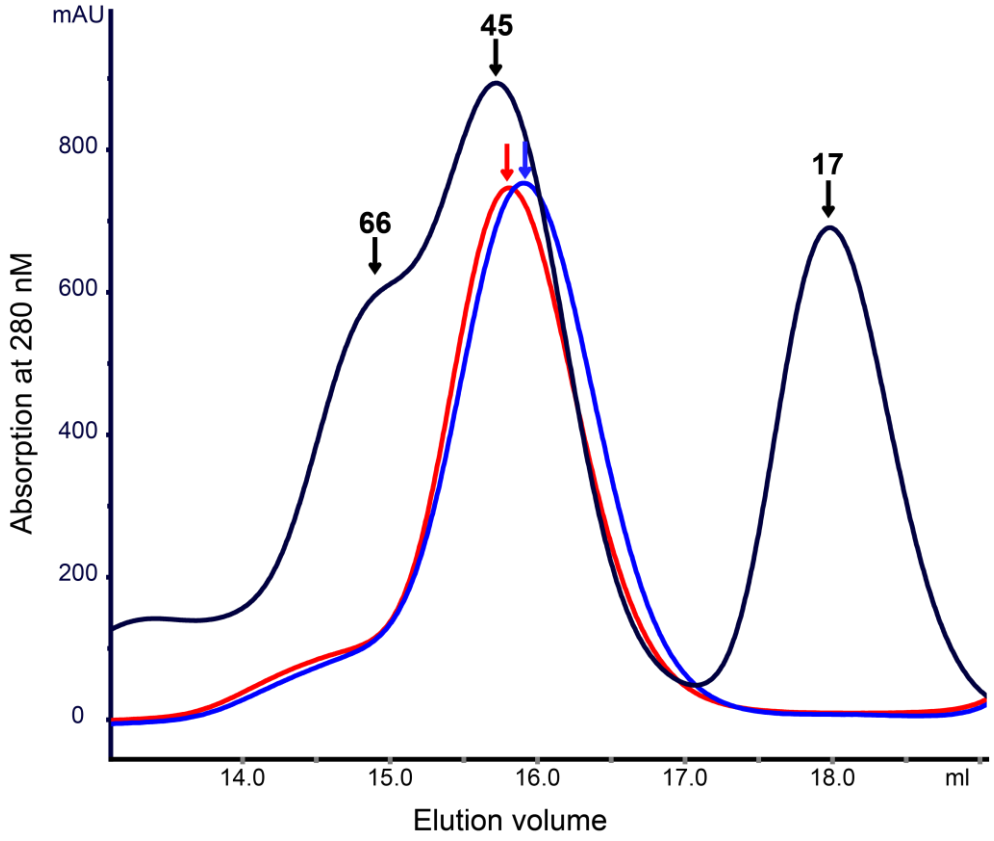

Fig. 3-8 Assembly state analysis of KetoC-bound CLA-ER by size-exclusion chromatography. The molecule-masses of markers are labeled above the peaks (kDa). The peaks of CLA-ERs in product-free state and KetoC-bound state are indicated by red and blue arrow, respectively.

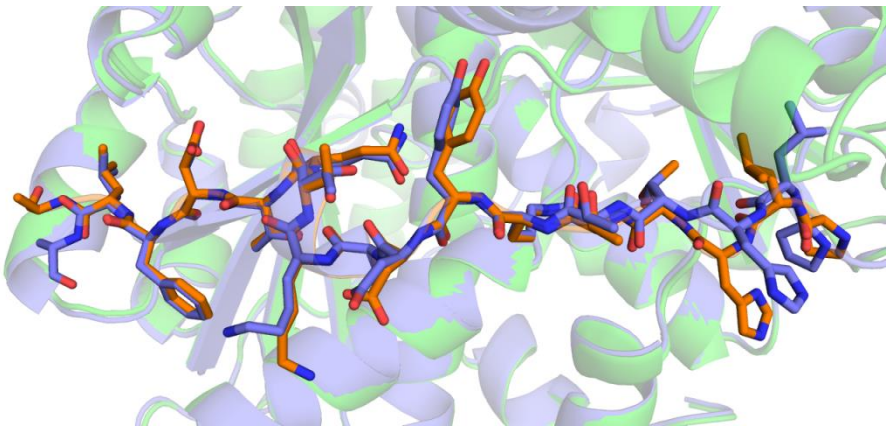

Fig. 3-9 Comparison of C-terminal tails in KetoC-bound state and product-free state. Structures of C-terminal tails in KetoC-bound and product-free state are colored in orange and slate, respectively.

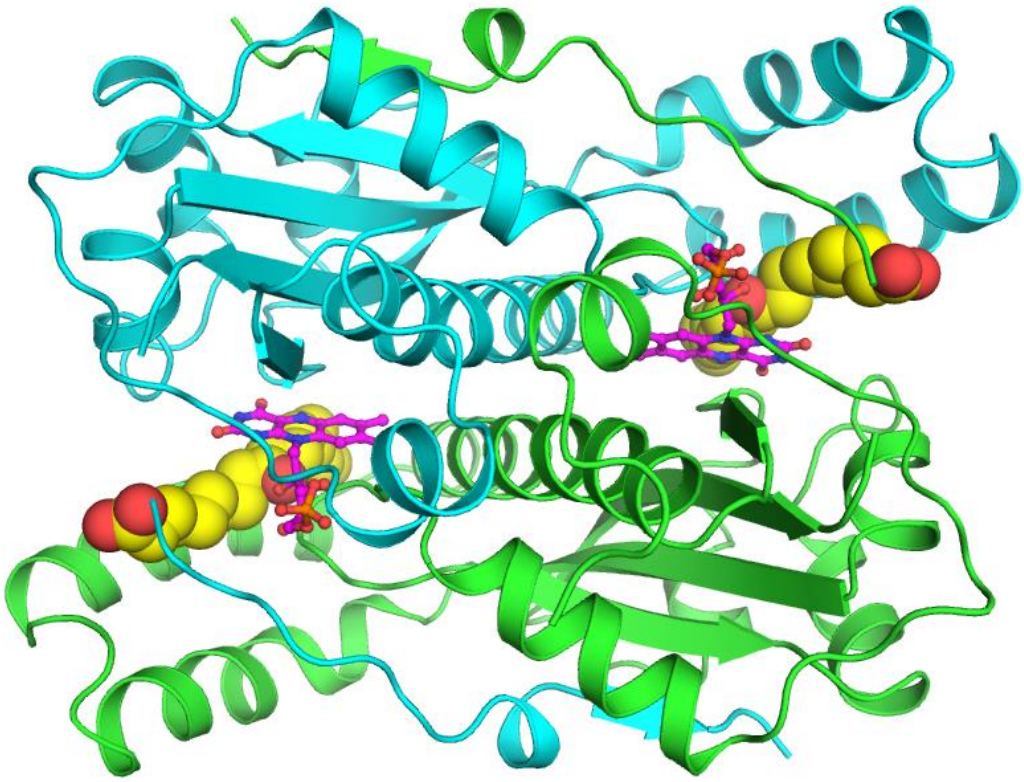

Fig. 3-10 Remodeled structure of CLA-ER in KetoC-bound state. Two protomers are colored differently. FMN and KetoC molecules are indicated by magentas stick-ball and yellow sphere model, respectively.

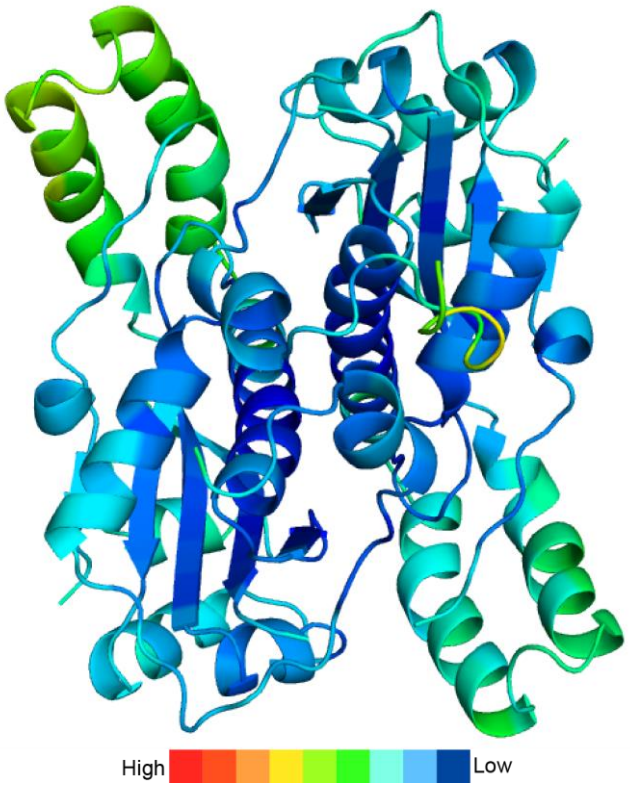

Fig. 3-11 Crystal structures of CLA-ER in KetoC-bound state colored by *B*-factor from blue (low) to red (high).

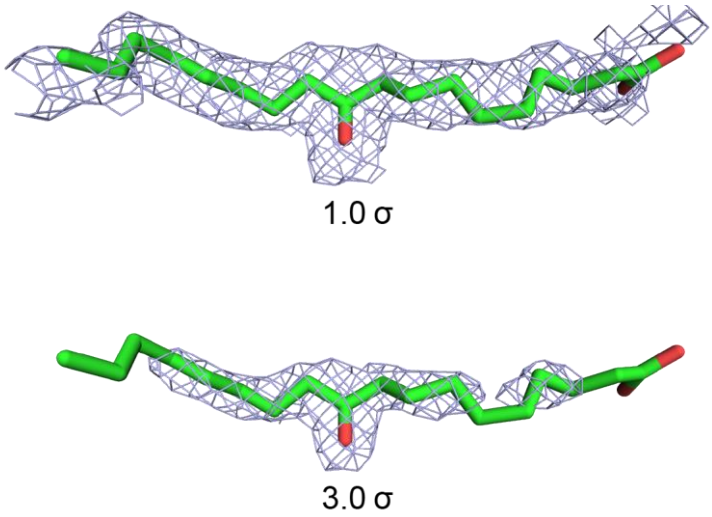

Fig. 3-12 $f_o - f_c$ electron density map for KetoC. KetoC molecules are indicated by green sticks.

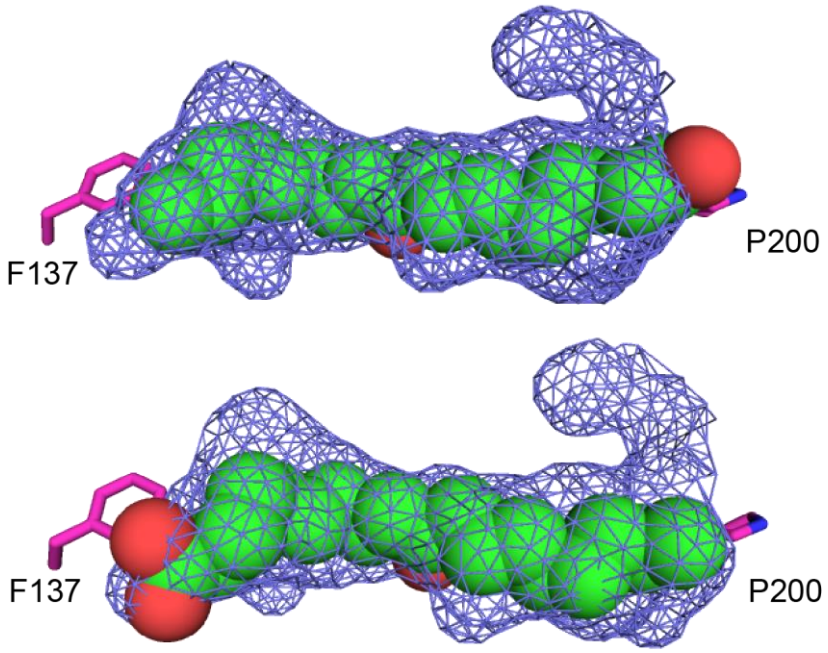

Fig. 3-13 Reversed binding model of KTC. The binding site is represented by slate mesh. Residues belonging to CLA-ER are indicated as magentas sticks. The KTC molecules are represented by green spheres.

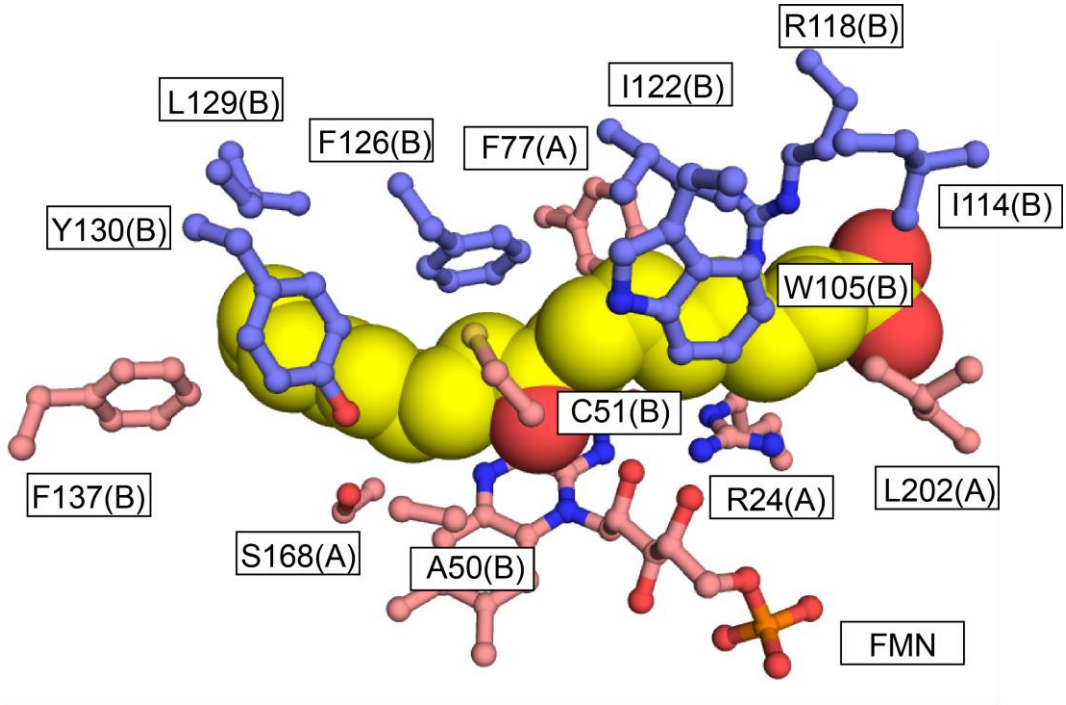

Fig. 3-14 Residues around KetoC. The residues belonging to the flexible subdomain are colored in slate and others are colored in wheat except KetoC molecule that is indicated by yellow sphere.

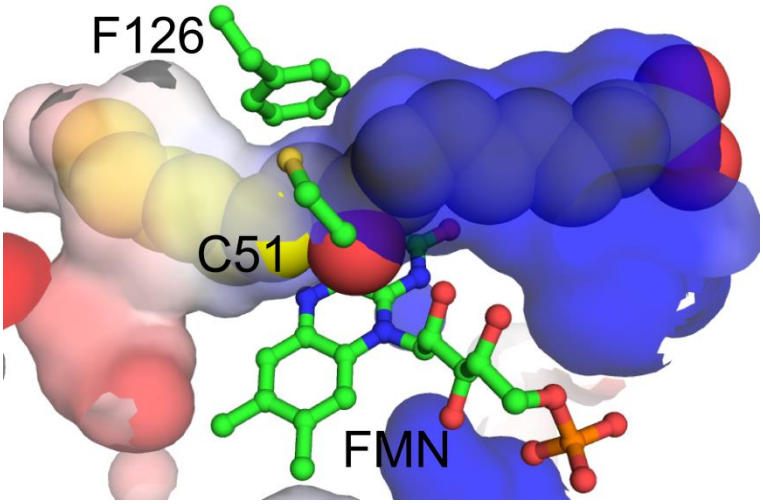

Fig. 3-15 Fatty acid binding tunnel in CLA-ER. Electrostatic surface potential of the tunnel is shown from red (negative charge) to blue (positive charge). FMN and residues at the middle region of the tunnel are highlighted by green stick. KetoC molecule is indicated by yellow sphere.

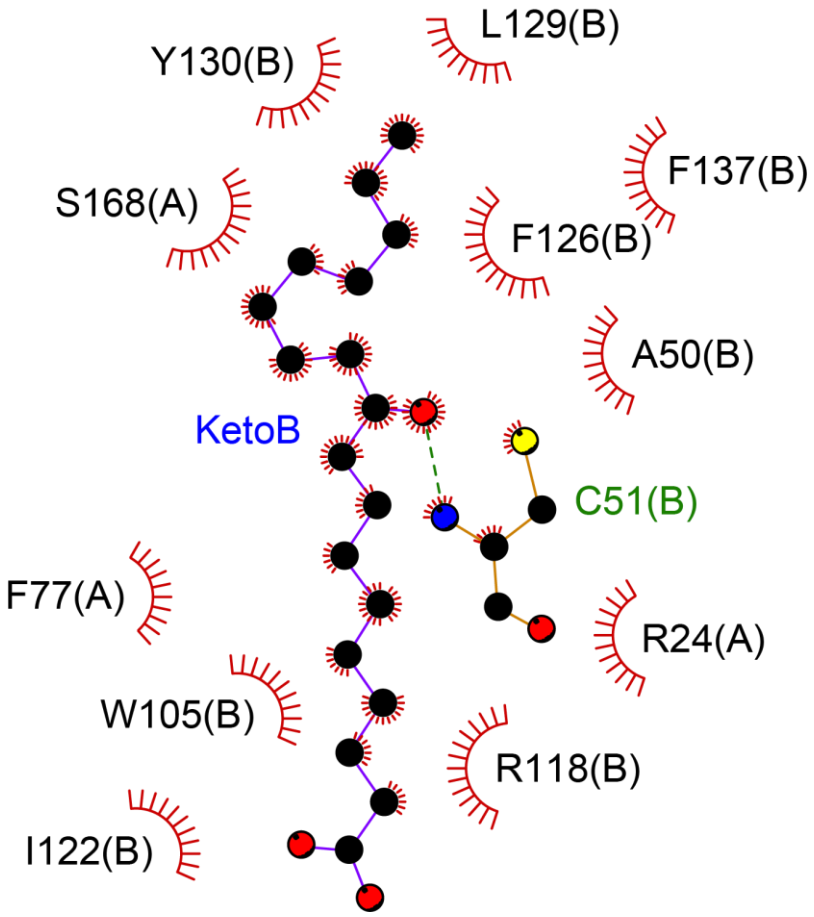

Fig. 3-16 Schematic representation for non-covalent interactions between KetoC and CLA-ER. Hydrogen bonds and hydrophobic interactions are indicated by green dashed line and red arc, respectively.

Chapter 4

Reaction mechanism of CLA-ER

4.1 Exordium

The structures of CLA-ER in the presence of both FMN and substrate/product have been determined successfully. Based on these structures, I analyzed the fatty-acid recognition mechanism of CLA-ER. However, it is still unknown how the tunnel formed and what happened during tunnel formation. Moreover, the critical residues for enoate reduction reaction and the reaction mechanism have not been clarified. In this chapter, structure comparison, mutational analysis and mechanism analysis will be described to explain the reaction mechanism of CLA-ER.

4.2 Material and methods

4.2.1 Preparation of mutation plasmids

The wild-type CLA-ER plasmids were used as template to produce a variety of mutants by site-directed mutagenesis: CLA-ER^{C51A}, CLA-ER^{C51S}, CLA-ER^{Y101F} and CLA-ER^{F126A}. All mutants were constructed using the Quickchange site-directed mutagenesis kit (Agilent Technologies) with primers listed in Table 4-1. The solution components and PCR process are as follows:

Reagent Composition for PCR	
10×Pfu buffer	5 μl
dNTPs	1 μl
Primers	1 μl
Template plasmid	0.5 μl
Pfu turbo	1 μl
MilliQ	41.5 μl

PCR process			
Step	Temperature (ºC)	Time (Sec)	Cycle
First denaturation	95	30	1
Denaturation	95	30	16
Annealing	55	60	
Extension	68	420	

The amplified plasmids were digested using restriction enzyme *Dpn*I at 37 ºC for 1 hr to remove the template plasmids. The leaving plasmids were transformed to XL1-Blue competent cell as described in Chapter 2. The plasmids extracted from cultured XL1-Blue cell were further verified using Fasmac DNA sequencing service.

4.2.2 Purification of enzymes for enzyme assay

Wild-type CLA-ER and its mutants are overexpressed in Rosetta(DE3) as described previously. Enzymes are simply purified using Ni-NTA superflow column. After dialysis against buffer containing 20 mM Tris-HCl (pH 8.0) and 100 NaCl, samples are concentrated using Vivaspin 20 (10,000 MWCO) and the concentration was measured by BCA protein assay.

4.2.3 Enzyme assay

Enzyme assay was performed in Kyoto University. Result of enzyme assay was provided by Prof. Ogawa's group.

4.3 Results and discussion

4.3.1 Superimposition of CLA-ER/FMN and CLA-ER/FMN/KetoC

Superposed structures in fatty acid-bound and fatty acid-free state reveal a completely same conformation of the core subdomain (RMSD of 0.315 Å). However, a significant conformational change was observed at the flexible subdomain. Upon KetoC binding, the flexible subdomain rotates about 45 deg towards the core subdomain of the other protomer in dimer (Fig. 4-1). The flexible subdomain acts as a "cap" to capture a fatty acid. The conformational change of the "cap" structure makes CLA-ER change to a closed form and results in the formation of a tunnel for fatty-acid recognition and reaction.

Insight into superposed structures also reveals that F126 undergoes an inversion of side chain followed by the conformational change of flexible subdomain. The inverted side chain of F126 acts as a "lock" to accurately fix spatial arrangement of the C=C group (Fig. 4-2). Additionally, an obvious movement of Y101 was also induced by the conformational change accompanying to KetoC binding. Y101 moved 8.4 Å towards active site to reside near C51 with a distance of 3.3 Å (Fig. 4-3). Y101 occupied the space of F126 and forced the rearrangement of F126. This observation reveals that the rearrangement of Y101 contributes to the spatial arrangement of F126 (Fig. 4-3).

4.3.2 Active site

Generally, the reaction of flavoenzyme is considered to proceed via the direct transfer of a hydride anion from flavin N5 to the substrate followed by protonation of the substrate from the opposite site residue or water molecule (57). In the structure of CLA-ER/KetoC, the N5 atom of flavin ring locates at the position of 3.1 Å from the C_{γ} atom corresponding to the C=C

group of substrate (Fig. 4-4), which is suitable for hydride anion transfer. Among the residues adjacent to the C=C group of substrate, C51 is the sole hydrophilic residue. Thus C51 may not only contribute to the spatial arrangement of C=C group but also play a key role in the protonation of substrate (Fig. 4-4). Two hydrophilic residues, Y101 and Y130, locate at 3.3 Å and 4.1 Å from C51, respectively (Fig. 4-4). A distance of 3.3 Å is suitable for hydrogen bond and electron transfer. However, a distance of 4.1 Å is too far.

4.3.3 Enzyme assay of CLA-ER mutants

To identify the critical residues for reaction, enzyme assay was performed with the site-directed mutants. The catalytic activity of CLA-ER was remarkably decreased by the F126A mutation, indicating that a “lock” residue is critical for the enoate reduction reaction (Fig. 4-5). C51 was also mutated to alanine and serine to investigate their influence in CLA-ER activity. As compared with the wild-type CLA-ER, activity of C51A mutants decreased to approximately 40% (Fig. 4-5), indicating that C51 is not essential for the activity of CLA-ER, but can facilitate the reaction. A mutation of C51 to serine residue does not affect the catalytic activity as compared with the wild-type CLA-ER (Fig. 4-5). The result suggests that a polar residue would improve the activity. Thus, C51 facilitates the reaction due to its polar feature, which may contribute to the electron transfer pathway. Y101F mutant also showed a significantly decreased activity (Fig. 4-5), indicating that Y101 is critical for the reaction. A distance of 3.3 Å from C51 indicates that Y101 may be also involved in the electron transfer pathway.

4.3.4 Proposed reaction mechanism

Based on crystal structure and the results of enzyme assay, I proposed the reaction

mechanism of CLA-ER. The enoate moiety of substrate was recognized by the hydrogen bonds with the amino group of C51 and the hydroxyl group of FMN, and hydrophobic interaction with the side chain of F126, resulting in C_γ atom at 3.1 Å from $FMNH^-$ N5 and C_β atom at 3.5 Å from thiol group of C51 residue (Fig. 4-2, 4-4). The C=C group of substrate was reduced by obtaining hydride from $FMNH^-$ N5 and proton from hydroxyl group of Y101 through the thiol group of C51 (Fig. 4-6A).

However, enzyme assay reveals that C51 is not an essential residue to reaction, which implies that there is another pathway for electron transfer. However, C51 is the sole hydrophilic residue adjacent to the C=C group. Therefore, I suppose that electron can also be transferred through the backbone of C51 and A50 to water molecule (Fig. 4-7). The water molecule interacts with several residues in both open and closed state, which indicates that it may play an important role in the reaction (Fig. 4-7). Similar pathway through backbone was also proposed on the proton transfer in cytochrome c oxidase (58). In this case, the first step of the reaction will result in an intermediate, which can transform to KetoC by itself in the following step (Fig. 4-6B). This electron transfer pathway help us to understand why the C51A mutants did not lose their activity but only showed decreased activities as compared with the wild type CLA-ER.

Table 4-1 Oligonucleotide used in site-direct mutation

Primer	Sequence
C51S_forward	5’ − GCCACCGCGCCATCGGCAAGCAATTTACAGTCATGGCAC − 3’
C51S_reverse	5’ − GTGCCATGACTGTAAATTGCTTGCCGATGGCGCGGTGGC − 3’
C51A_forward	5’ − CCACCGCGCCATCGGCAGCGAATTTACAGTCATGGC − 3’
C51A_reverse	5’ − GCCATGACTGTAAATTCGCTGCCGATGGCGCGGTGG − 3’
F126A_forward	5’ − CTTGGATCAGATTCTGGGAACCGCGTTACCATTATATGAAAATGCC − 3’
F126A_reverse	5’ − GGCATTTTCATATAATGGTAACGCGGTTCCCAGAATCTGATCCAAG − 3’
Y101F_forward	5’ − CCCAGTCGCATTATGTTTTCCGCGATGTCTGGAACAAAG − 3’
Y101F_reverse	5’ − CTTTGTTCCAGACATCGCGGAAAACATAATGCGACTGGG − 3’

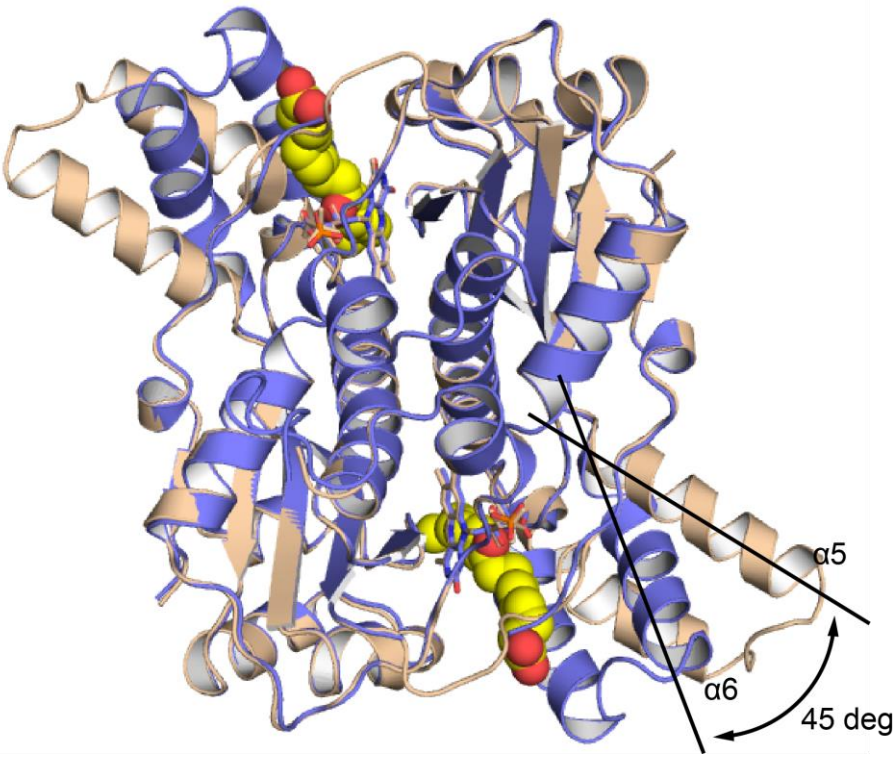

Fig. 4-1 Superimposition of CLA-ERs with and without fatty acid binding. The structures of CLA-ER/FMN and CLA-ER/FMN/KetoC are colored in wheat and slate, respectively. FMN and KetoC molecules are indicated as stick and sphere, respectively.

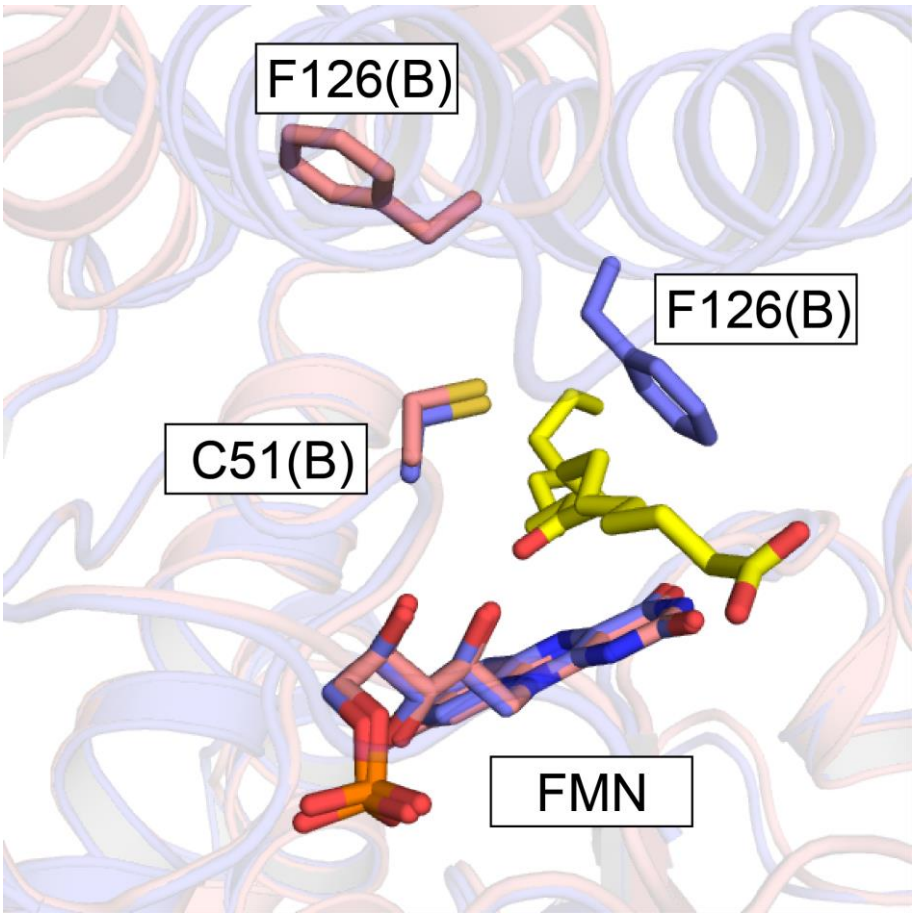

Fig. 4-2 Conformational change of F126. The structures of CLA-ER/FMN and CLA-ER/FMN/KetoC are colored in pink and slate, respectively.

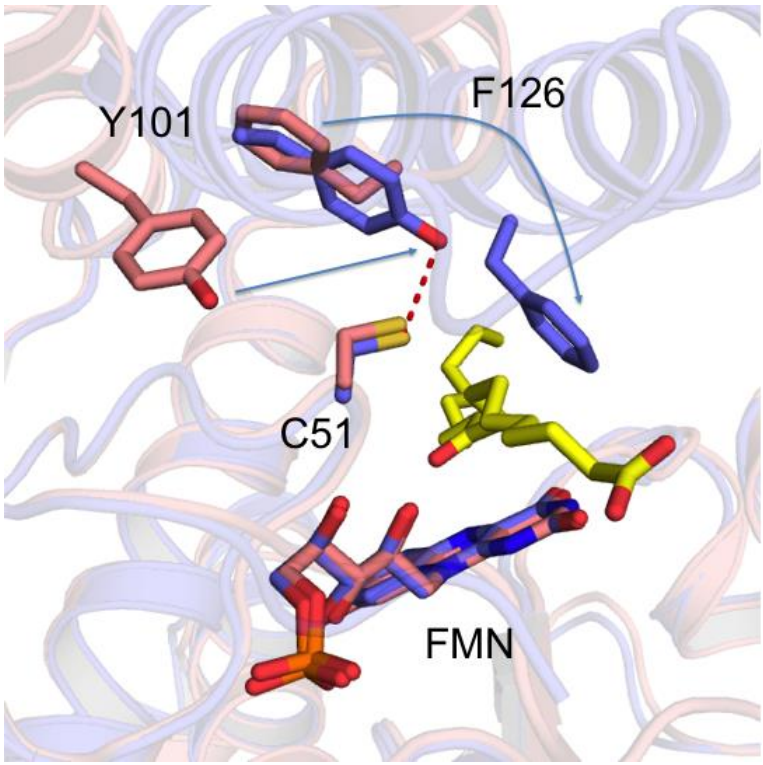

Fig. 4-3 Conformational change of Y101. The structures of CLA-ER/FMN and CLA-ER/FMN/KetoC are colored in pink and slate, respectively.

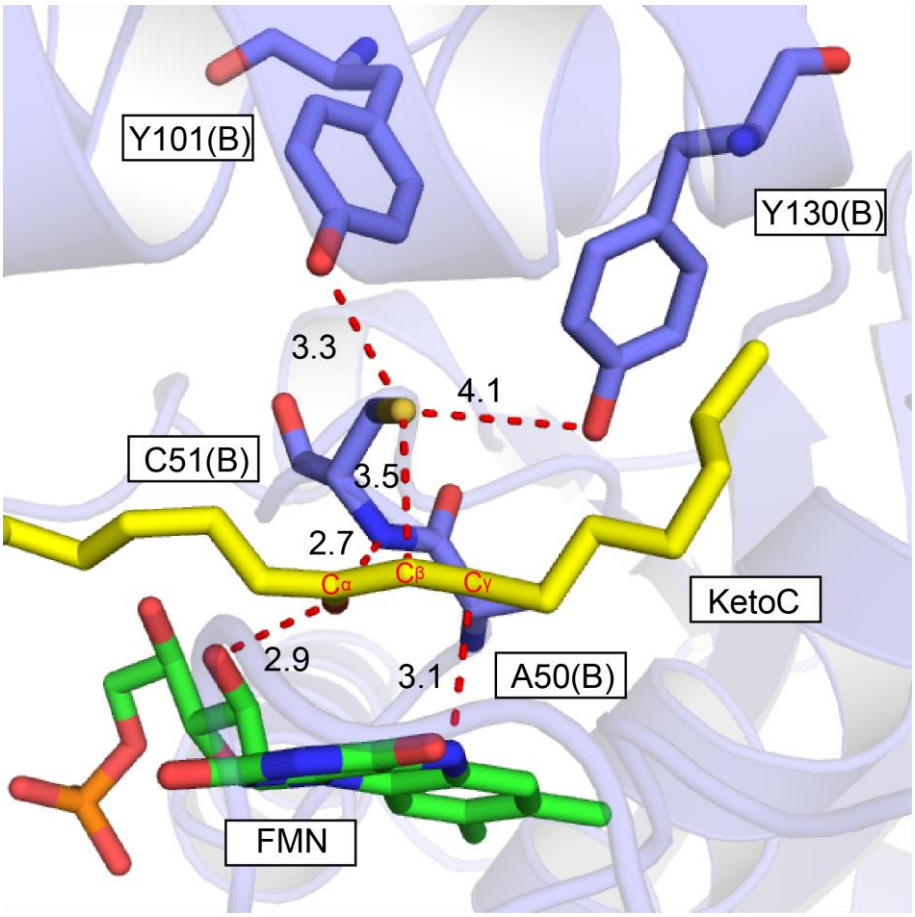

Fig. 4-4 Active site of CLA-ER. Residues and molecules maybe involved in electron transfer are presented by stick.

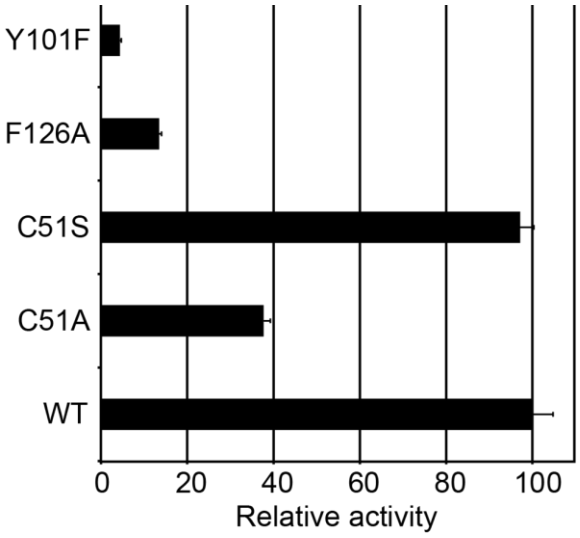

Fig. 4-5 Enoate reduction activities of wild-type CLA-ER and its mutants.

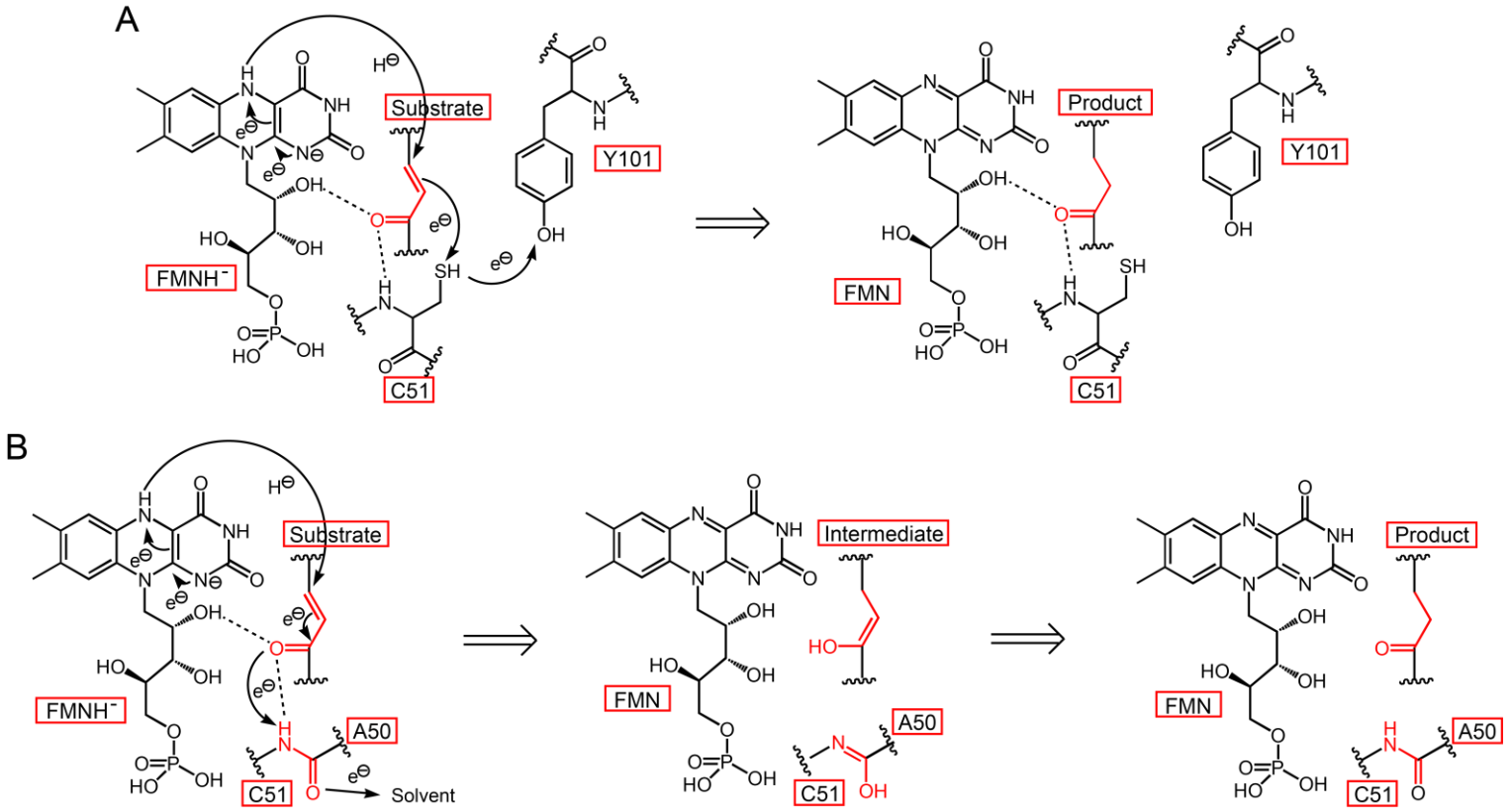

Fig. 4-6 Schematic program of reaction mechanism of CLA-ER. Electron transfer pathway is indicated by black arrows. Enoate moiety of fatty acid and amino acid backbones involved in the electron transfer are highlighted in red.

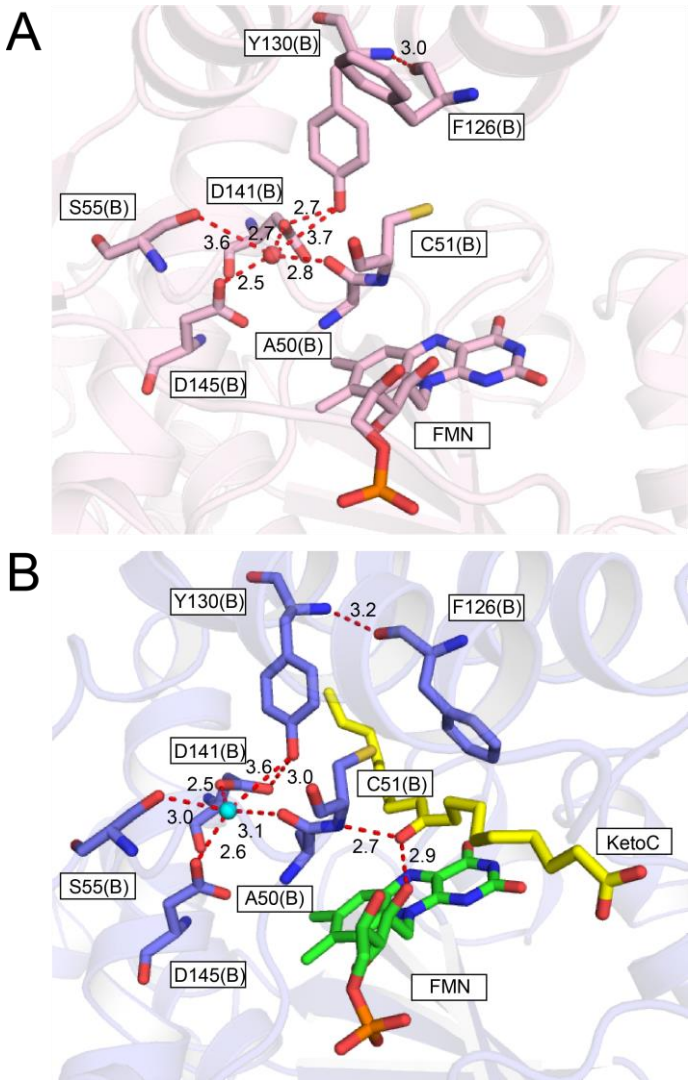

Fig. 4-7 Residues and water molecule involved in the candidate pathway. Water molecule is indicated as cyan sphere. (A) CLA-ER/FMN. (B) CLA-ER/FMN/KetoC

Chapter 5

General discussion

5.1 Enzymes in NADH oxidase/flavin reductase family

Although enzymes belonging to NADH oxidase/flavin reductase family have been extensively studied, there are rarely reports on enzymes showing enoate reduction activity. Therefore, I try to explain the reason for the novel activity of CLA-ER. Enzymes with similar structure to CLA-ER were searched using DALI (59). By comparison of these enzymes, I found that the "cap" structure in CLA-ER is not conserved in all these enzymes. I termed enzymes containing a "cap" structure as group I, enzymes only contains the central conserved domain as group II, and enzymes have other character structures as others (Fig. 5-1, 5-2). As described in reaction mechanism, the "cap" structure contains a hydrophobic residue (F126) critical for the spatial arrangement of C=C group and a tyrosine residue (Y101) involved in both electron transfer and rearrangement of F126. Therefore, a "cap" structure is considered to be essential for the enoate reduction reaction. Deletions of this "cap" structure in enzymes in other groups may lead to the loss of enoate reduction activities. In group I, 14 structures have been determined and contain a "cap" structure. Alignment of the amino acid sequence reveals that none of these enzymes conserved both the catalytic cysteine and tyrosine residues (Fig. 5-3). Particularly, the cysteine residue in the active site was not found in any of these enzymes (Fig. 5-3). The activities of cysteine mutants have been demonstrated to decrease remarkably. Therefore, the deletion of cysteine residue may make the enoate reduction activity difficult to be identified. With all mentioned above, both the "cap" structure with a hydrophobic "key" and the catalytic cysteine, tyrosine residues are considered to be the structural features that allow CLA-ER identified as an enoate reductase preferentially.

I also aligned the sequences of enzymes with different sequence identities to CLA-ER (Fig. 5-3). The result shows that F126 are well conserved in most of these enzymes, but Y101 and C51 are only conserved in the enzymes with identities above 49%. Therefore, I speculate that enzymes with identities of more than 49% may also have potential to catalyze an enoate

reduction reaction.

5.2 Recognition of fatty acids without CoA- or ACP-activation

Activations of fatty acid by linking to CoA or ACP are considered to be helpful in further modification. These carriers not only make fatty acid easily transferred to other molecules, but also contribute to the recognition of acyl group. In the structure of mDECR complexed with *trans*-2,*trans*-4-hexdienoyl-CoA, CoA moiety forms several hydrogen bonds with water molecules and side-chain functional groups, which contributes to the special arrangement of dienoyl group for saturation reaction (Fig. 5-4) (60). Structure analysis of other enoate-CoA reductases using docking modeling also indicates that the CoA group interacts extensively with enzymes and contributes to substrate recognition (61, 62). On the other hand, study on ACP bound to FabI reveals that the complex is primarily stabilized by interactions between acidic residues in the ACP and substrate-binding loop in the FabI. By these interactions, ACP is able to successfully deliver the substrate into the FabI active site through a minor portal (42).

Strikingly, CLA-ER catalyzes enoate reduction reaction on fatty acids without CoA or ACP carrier binding. As described in Chapter 2, CLA-ER adopts an open form in fatty acid-free state, which results in exposure of the groove for preliminary recognition of fatty acid (Fig. 5-5). The open form of CLA-ER allows its substrate to approach the binding groove without the help of carrier. Additionally, the charge distribution of the groove contributes to the orientation of substrate (Fig. 5-5). The positive charges induce the recognition of carboxyl group of fatty acid. Substrate is further recognized by the hydrogen bonds of substrate−FMN and substrate−C51, and the large conformational change in the “cap” structure. Therefore, both the charge distribution of the groove and transformation of open-closed structures make the substrate recognition possible without the combination with CoA or ACP. These features

enable CLA-ER to reduce fatty acids that are difficult to link to CoA or ACP.

5.3 Perspective

In this work, the crystal structure of CLA-ER was determined. Based on the structural and mutational analysis, I elucidated the mechanisms of substrate recognition and enoate reduction reaction. Although 10-oxo-*trans*-11-octadecenoic acid was used as substrate of CLA-ER, the sandglass shape of catalytic site and open channel on both ends allow possibilities that CLA-ER may catalyze the enoate reduction reaction on fatty acids with different lengths (Fig. 5-6). Therefore, further studies will be expected on the diversity of substrate.

On the other hand, the structure, substrate recognition mechanism and reaction mechanism of leaving three enzymes involved in the novel linoleic acid saturation pathway are still unknown. To elucidate the pathway completely, further studies will be expected on structures of these enzymes. All these enzymes are extensively conserved in lactic acid bacteria that are widely distributed in GI-tract and influence the fatty acid metabolism in their host. Therefore, research on these enzymes will not only expand our understanding on fatty acid metabolic pathway, but also may offer new opportunities for the development of health food and drug.

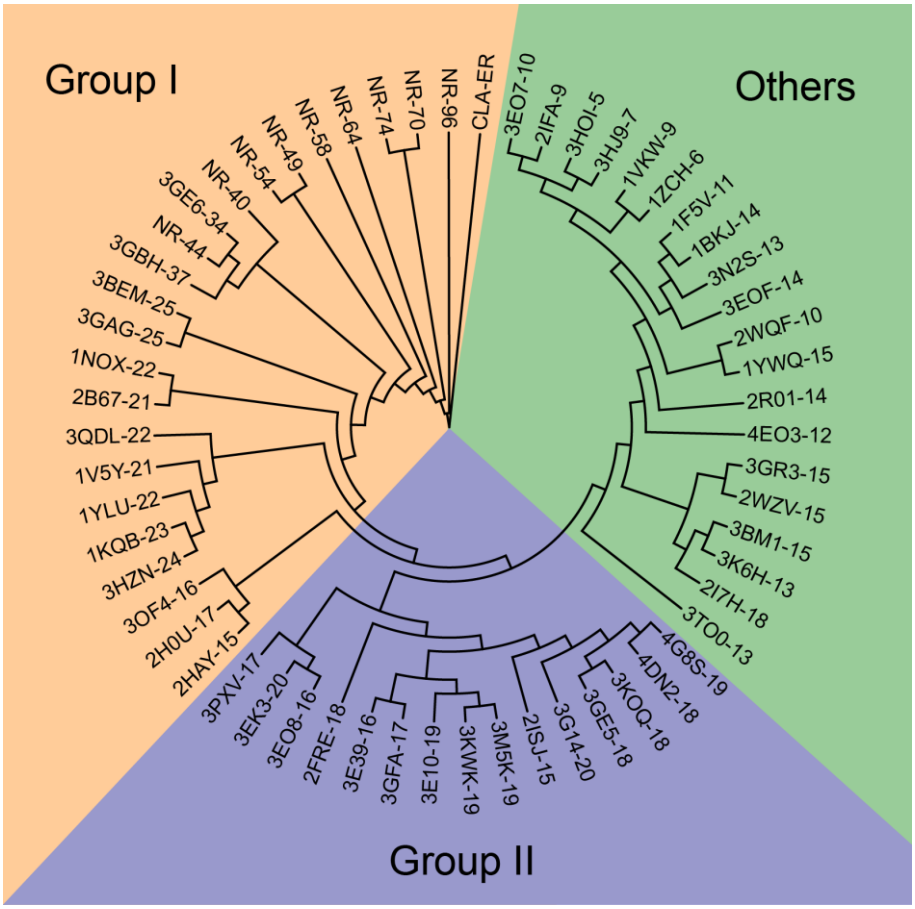

Fig. 5-1 Phylogenetic tree of enzymes with a structure similar to CLA-ER. Enzymes are divided into three groups termed Group I, Group II and Others and colored by wheat, slate and palegreen, respectively.

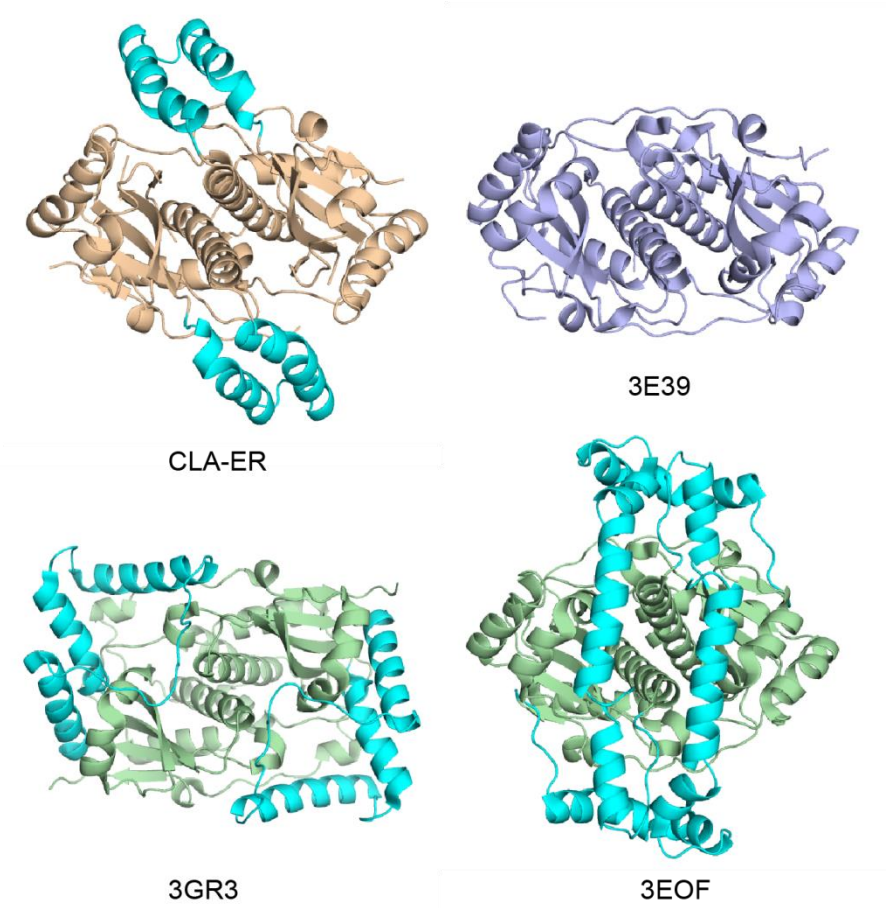

Fig. 5-2 Crystal structures of some enzymes in NADH oxidase/flavin reductase family. Conserved domains are colored according to their groups in Fig. 5-1. Diverse domains are highlighted in cyan.

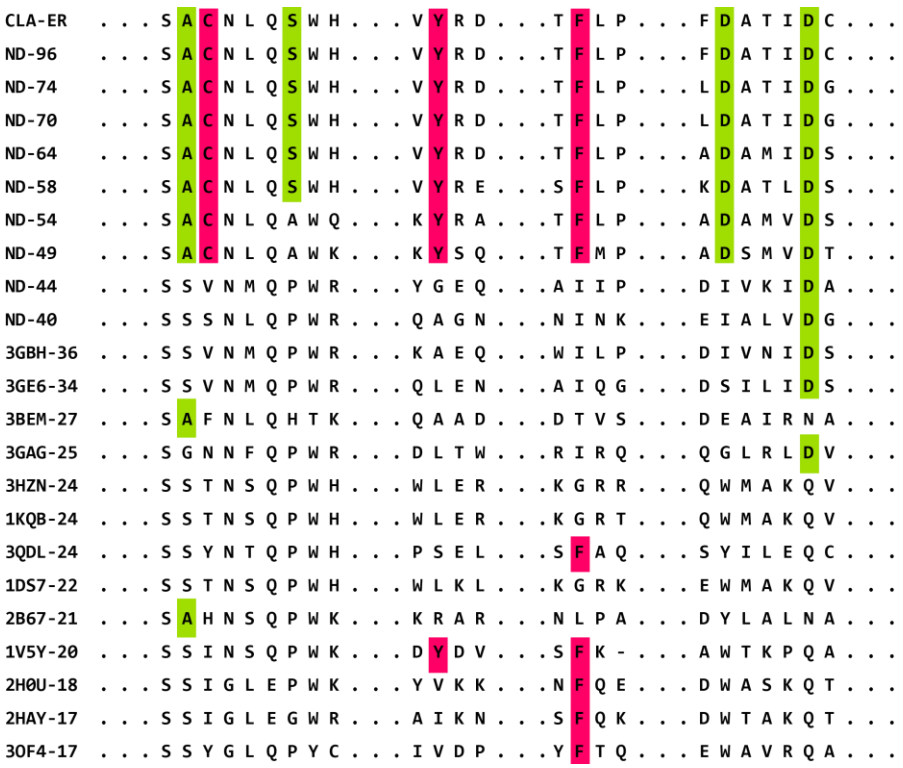

Fig. 5-3 Sequence alignment of CLA-ER-like enzymes. Critical residues are indicated by small colored block.

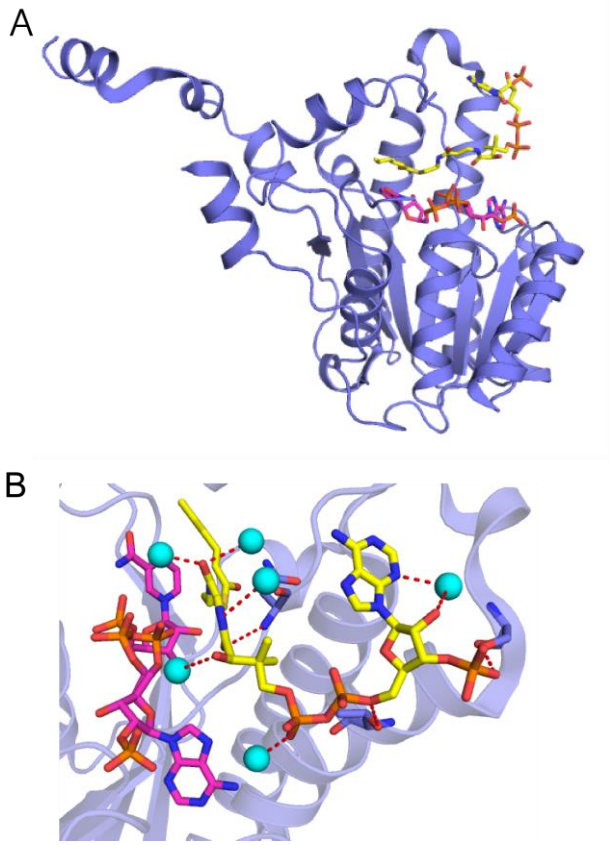

Fig. 5-4 The crystal structure of mDECR complex with *trans*-2,*trans*-4-hexdienoyl-CoA. NADPH, substrate and water molecules are indicated by magentas stick, yellow stick and cyan sphere, respectively.

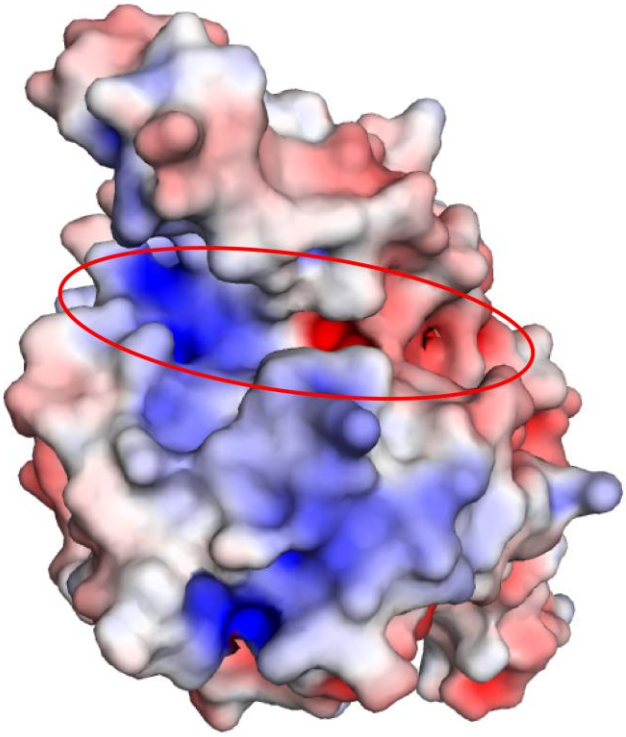

Fig. 5-5 Electrostatic surface potential of CLA-ER in open state. The groove for fatty acid binding is indicated by red ellipse.

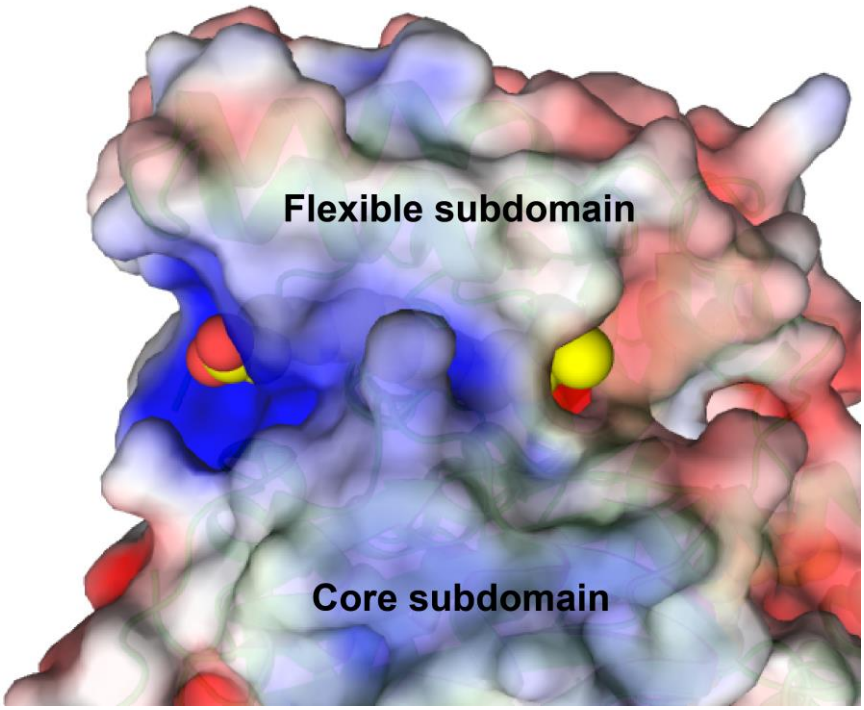

Fig. 5-6 Tunnel for fatty acid binding.

Reference

(1) Haunerland NH, Spener F (2004) Fatty acid-binding proteins-insights from genetic manipulations. *Prog Lipid Res* 43(4):328-349

(2) Chmurzynska A (2006) The multigene family of fatty acid-binding proteins (FABPs): function, structure and polymorphism. *J Appl Genet* 47(1):39-48

(3) Makowski L, hotamisligil GS (2005) The role of fatty acid binding proteins in metabolic syndrome and atherosclerosis. *Curr Opin Lipidol* 16(5):543-548

(4) Coe NR, Bernlohr DA (1998) Physiological properties and functions of intracellular fatty acid-binding proteins. *Biochim Biophys Acta* 1391(3):287-306

(5) Zimmerman AW, Veerkamp JH (2002) New insights into the structure and function of fatty acid-binding proteins. *Cell Mol Life Sci* 59(7):1096-1116

(6) Xu A, et al. (2006) Adipocyte fatty acid-binding protein is a plasma biomarker closely associated with obesity and metabolic syndrome. *Clin. Chem.* 52(3):405-413

(7) Tso AW, et al. (2007) Serum adipocyte fatty acid binding protein as a new biomarker predicting the development of type 2 diabetes: a 10-year prospective study in a Chinese cohort. *Diabetes Care* 30(10):2667-2672

(8) Yeung DC, et al. (2007) Serum adipocyte fatty acid-binding protein levels were independently associated with carotid atherosclerosis. *Arterioscler Throm. Vasc. Biol.* 27(8):1796-1802

(9) Kralisch S, Fasshauer M (2013) Adipocyte fatty acid binding protein: a novel adipokine involved in the pathogenesis of metabolic and vascular disease. *Diabetologia* 56(1):10-21

(10) Tvrzicka E, Kremmyda LS, Stankova B, Zak A (2011) Fatty acids as biocompounds: their role in human metabolism, health and disease—a review. Part 1: classification, dietary sources and biological functions. *Biomed Pap Med Fac Univ Palacky Olomouc Czech Repub* 155(2):117-30

(11) Kremmyda LS, Tvrzicka E, Stankova B, Zak A (2011) Fatty acids as biocompounds: their role in human metabolism, health and disease—a review. Part 2: fatty acid physiological roles and applications in human health and disease. *Biomed Pap Med Fac Univ Palacky Olomouc Czech Repub* 155(3):195-218

(12) Watkins PA (1997) Fatty acid activation. *Prog Lipid Res* 36(1):55-83

(13) Schweizer E, Höfmann J (2004) Microbial type I fatty acid synthases (FAS): major player in a network of cellular FAS systems. *Microbiol Mol Biol Rev* 68(3):501-507

(14) Leonard AE, Pereira SL, Sprecher H, Huang YS (2004) Elongation of long-chain fatty acids. *Prog Lipid Res* 43(1):36-54

(15) Jakobsson A, Westerberg R, Jacobsson A (2006) Fatty acid elongases in mammals: their regulation and roles in metabolism. *Prog Lipid Res* 45(3):237-249

(16) Hitunen JK, et al. (2009) Mitochoondrial fatty acid synthesis type II: more than just fatty acids. *J Biol Chem* 284(14):9011-9015

(17) Smith S (1994) The animal fatty acid synthase: one gene, one polypeptide, seven enzymes. *FASEB J* 8(15):1248-1259

(18) Osei P, et al. (1988) Topography of rat hepatic microsomal enzymatic components of the fatty acid chain elongation system. *J Biol Chem* 264(2):6844-6849

(19) Kishino S, Ogawa J, Ando A, Shimizu S (2003) Conjugated α-linolenic acid by *Lactobacillus plantarum* AKU 1009a. *Eur J Lipid Sci Technol* 105(10):572-577

(20) Ogawa J, et al. (2005) Production of conjugated fatty acids by lactic acid bacteria. *J Biosci Bioeng* 100(4):355-364

(21) Ogawa J, et al. (2006) Screening and industrial application of unique microbial reactions involved in nucleic acid and lipid metabolisms. *Biosci Biotechnol Biochem* 70(3):574-582

(22) Kishino S, Ogawa J, Yokozeki K, Shimizu S (2009) Metabolic diversity in biohydrogenation of polyunsaturated fatty acid bacteria involving conjugated fatty acid production. *Appl Microbiol Biotechnol* 84(1):87-97

(23) Kishino S, OgawaJ, Ando A, yokozeki K, Shimizu S (2010) Microbial production of conjugated γ-linolenic acid by *Lactobacillus plantarum* AKU 1009a. *J Appl Microbiol* 108(6):2012-2018

(24) Kishino S, et al. (2013) Polyunsaturated fatty acid saturation by gut lactic acid bacteria affecting host lipid composition. *Proc Natl Acad Sci U S A* 110(44):17808-17813

(25) Round JL, Mazmanian SK (2009) The gut microbiota shapes intestinal immune responses during health and disease. *Nat Rev Immunol* 9(5):313–323

(26) Polan CE, McNeill JJ, Tove SB (1964) Biohydrogenation of unsaturated fatty acids by rumen bacteria. *J Bacteriol* 88(4):1056–1064.

(27) Stiles ME, Holzapfel WH (1997) Lactic acid bacteria of foods and their current taxonomy. *Int J Fool Microbioli* 36(1):1-29

(28) Tannock GW (2004) A special fondness for Lactobacilli. *Appl Environ Mircrobiol* 70(6):3189-3194

(29) Johansson ML, et al. (1998) Survival of *Lactobacillus plantarum* DSM 9843 (299v), and effect on the short-chain fatty acid content of faeces after ingestion of a rose-hip drink with fermented oats. *Int J Food Microbiol* 42(1-2), 29-38

(30) Cunningham-Rundles S, et al. (2000) Probiotics and immune response. *Am J Gastroenterol* 95(1):S22-S25

(31) Pariza MW, Ha YL (1990) *Antimutagenesis and Anti carcinogenesis Mechanism II*, eds Kuroda Y, shankel D, Waters MD (Plenum, New York), pp 167-170

(32) Lee KN, Kritchevsky D, Pariza MW (1994) Conjugated linoleic acid and atherosclerosis in rabbits, Atherosclerosis 108(1):19-25

(33) Park Y, et al. (1997) Effect of conjugated linoleic acid on body composition in mice. *Lipids* 32(8):853-858

(34) Terés S, et al. (2008) Oleic acid content is responsible for the reduction in blood pressure induced by olive oil. *Proc Natl Acad Sci U S A* 105(37):13881-13886

(35) Food and Nutrition Board, Institute of Medicine (2005) *Dietary Reference Intakes for Energy, Carbohydrte, Fiber, Fat, Fatty acids, Cholesterol, Protein, and Amino Acids* (National Academies Press, Washington, DC), pp 422-541

(36) Itoh T, et al. (2008) Structural basis for the activation of PPARγ by oxidized fatty acids. *Nat Struct Mol Biol* 15(9):924-931

(37) Kim YI, et al. (2012) Potent PPAR activator derived from tomato juice, 13-oxo-9,11-ictadecadienoic acid, decreases plasma and hyepatic triglyceride in obese diabetic mice. *PloS ONE* 7(2):e31317

(38) Parkinson GN, Skelly JV, Neidle Stephen (2000) Crystal structure of FMN-dependent nitroreductase from *Escherichia coli* B: a prodrug-activating enzyme. *J. Med. Chem.* 43(20):3624-3631

(39) Race PR, et al. (2005) Structural and mechanistic studies of *Escherichia coli* nitroreductase with the antibiotic nitrofurazone. *J. Biol. Chem.* 280(14):13256-13264

(40) Thomas SR, McTamney PM, Adler JM BaRonde-LeBlanc N, Rokita SE (2009) Crystal structure of lodotyrosine deiodinase, a novel flavoprotein responsible for iodide salvage in thyroid glands. *J. Biol. Chem.* 284(29):19659-19667

(41) Taga ME, et al. (2007) BluB cannibalizes flavin to form the lower ligand of vitamin B_{12}. *Nature* 446(7134):449-453

(42) Rafi S, et al. (2006) Structure of acyl carrier protein bound to FaBI, the FASII enoyl reductase from *Escherichia coli. J. Biol. Chem.* 281(51):39285-39293

(43) Saito J, et al. (2008) Crystal structure of enoyl-acyl carrier protein reductase (FabK) *Streptococcus pneumoniae* reveals the binding mode of an inhibitor. *Protein Sci.* 17(4):691-699

(44) Kohli RM, Massey V (1998) The oxidative half-reaction of old yellow enzyme. *J. Biol Chem.* 270(49):32763-32770

(45) Ames BD, et al. (2012) Crystal structure and biochemical studies of the trans-acting

polyketide enoyl reductase LovC from lovastatin biosynthesis. *Proc. Natl. Acad. Sci. U. S. A.* 109(28):11144-11149

(46) Smith PK, et al. (1987) Measurement of protein using bicinchoninic acid. *Anal Biochem* 150(1):76-85

(47) Kabsch W (2010) Integrating, scaling, space-group assignment and post-refinement. *Acta Crystallogr D Biol Crystallogr* 66(Pt 2):133-144.

(48) Matthews BW (1968) Solvent content of protein crystals. *J. Mol. Biol.* 33(2):491-497

(49) Vagin A, Teplyakov A (2000) An approach to multi-copy search in molecular replacement. *Acta Crystallogr D Biol Crystallogr* 56(Pt 12):1622–1624.

(50) Adams PD, et al. (2010) PHENIX: a comprehensive python-based system for macromolecular structure solution. *Acta Crystallogr D Biol Crystallogr* 66(Pt 2):213-221

(51) Emsley P, Cowtan K (2004) Coot: Model-building tools for molecular graphics. *Acta Crystallogr D Biol Crystallogr* 60(Pt 12 Pt 1):2126-2132

(52) Lovell SC, et al. (2003) Structure validation by calpha geometry: phi, psi and cbeta deviation. *Proteins* 50(3):437-450

(53) DeLano WL (2002) The PyMOL Molecular Graphics System, http://www.pymol.org

(54) Laskowski RA, Swindells MB (2011). LigPlot+: multiple ligand-protein interaction *diagrams for drug discovery. J. Chem. Inf. Model. 51(10):2778-2786*

(55) Larkin MA, et al (2007) Clustal W and Clustal X version 2.0. *Bioinformatics* 23(21):2947-2948.

(56) Perrakis A, Harkiolaki M, Wilson K, Lamzin V (2001) ARP/wARP and molecular replacement. *Acta Crystallogr D Biol Crystallogr* 57(Pt 10):1445-1450

(57) Breithaupt C, et al (2001) X-ray structure of 12-oxophytodienoate reductase 1 provides structural insight into substrate binding and specificity within the family of OYE. *Structure* 9(5):419-429

(58) Thomas SR, McTamney PM, Adler JM BaRonde-LeBlanc N, Rokita SE (2009) Crystal

structure of lodotyrosine deiodinase, a novel flavoprotein responsible for iodide salvage in thyroid glands. *J. Biol. Chem.* 284(29):19659-19667

(59) Holm L, Rosenstrom P (2010) Dali server: conservation mapping in 3D. *Nucleic Acids Res* 38(Web server issue):W545-W549.

(60) Alphey MS, Yu W, Byres E, Li D, Hunter WN (2005) Structure and reactivity of human mitochondrial 2,4-dienoyl-CoA reductase. *J Biol Chem* 280(4):3068-3077

(61) HU K, et al. (2013) Structures of *trans*-2-enoyl reductases from *Clostridium acetobutylicum* and *Treponema denticola*: insights into substrate specificity and the catalytic mechanism. *Biochem J* 449(1):79-89

(62) Bond-Watts BB, Weeks AM, Chang MCY (2012) Biochemical and structural characterization of the *trans*-enoyl-CoA reductase from *Treponema denticola*. *Biochemstry* 51(34):6827-6837

Acknowledgements

First of all, I am deeply indebted to my supervisor, Prof. Masaru Tanokura, who gave me this opportunity to develop my academic career in the University of Tokyo. I received many helpful comments and advice not only with regard to my research but also on how to become a good researcher.

I would like to express my sincere thanks to Prof. Jun Ogawa and assistant professor Shigenobu Kishino at the graduate school of agriculture, Kyoto University, for collaborative research on enzyme assay.

I am deeply grateful to my team leader, assistant professor Takuya Miyakawa in the Tanokura's laboratory, for teaching me various techniques as well as philosophy that a crystallographer should be acquainted with.

I would like to thank Dr. Akira Nakamura in the Tanokura' laboratory for discussing with me whenever I need to. He gave me much valuable advice to advance my research.

I would also like to thank all the members in the Tanokura's laboratory and my families for their continuous support and encouragement.